Original article

Green synthesis of magnetic biochars derived from biobased orange peel materials as sustainable heterogeneous catalytic supports for the Fenton process

Georges Teikam Kenda [a], Paul Alain Nanssou Kouteu [b,c], Donald Raoul Tchuifon Tchuifon [a,b,*], Cyrille Ghislain Fotsop [a,d], Aurelien Bopda [a], Herman-Idriss Tiotsop Kuete [a], Nche George Ndifor-Angwafor [a], Solomon Gabche Anagho [a,*]

[a] Department of Chemistry, Research Unit of Noxious Chemistry and Environmental Engineering. Faculty of Science, University of Dschang, P.O. Box 67, Dschang, Cameroon
[b] Department of Process Engineering, Laboratory of Energy, Materials, Modeling and Method, National Higher Polytechnic School of Douala, University of Douala, P.O. Box 2701, Douala, Cameroon
[c] Process Engineering Laboratory, Ucac-Icam Institute, P.O. Box 5504, Douala, Cameroon
[d] Institute of Chemistry, Faculty of Process and Systems Engineering, Universität Platz 2, 39106 Magdeburg, Germany

ARTICLE INFO

ABSTRACT

In this work, two magnetite-biochar composite materials obtained via hydrothermal and co-precipitation methods to degrade dyes were evaluated. The two composite materials alongside their biochar precursor were characterized by X-ray diffraction (XRD), Fourier-transform infrared (FT-IR) spectroscopy, electrochemical impedance spectroscopy (EIS), scanning electron microscopy (SEM), energy dispersive spectroscopy (EDX), Raman spectroscopy and N_2 adsorption–desorption studies. Results of characterization showed a change in the amorphous structure of the biochar to a crystalline form after modification by both methods, the incorporation of magnetic particles into the carbonaceous matrix of the biochar precursor. In addition, the effect of solution pH, initial dye concentration H_2O_2 concentration, mass of composite material and the time of stirring on dye degradation were analysed by the response surface methodology. Both materials demonstrate appreciable stability over repeated cycles and more interestingly, Fe_3O_4-BC2 retains its catalytic efficiency much more than Fe_3O_4-BC1. Statistical analysis of the degradation results by ANOVA revealed a good correlation between the five parameters and the expected response with coefficients of correlation very close to unity. The degradation of reactive red-198 in the presence of both materials is best described by the second order kinetic rate law.

1. Introduction

Water is one of the most essential and indispensable elements of life. Increase in industrial activities bring about a degradation of the quality and quantity of water reserves in the world. These activities generate chemical substances that interfere with the geochemical cycle of water and lead to a deterioration of water quality. Textile industries frequently discharge their waste into the environment without prior proper treatment. Pollution of water sources by dyes is becoming a major environmental problem since these colouring agents can cause significant damage to both human health and aquatic organisms. These dyes are highly toxic, carcinogenic, mutagenic, teratogenic, and stable during aerobic degradation (Gupta et al., 2013). Due to the presence of aromatic rings and —N≡N— bonds in their structures, reactive dyes specifically are considered as recalcitrant xenobiotic organic pollutants (Raghavan et al., 2013). Another issue of great concern posed by this class of dyes is the fact that they have low fixation rates with fibre and this means about 10–20 % of the total dye used in the dyeing process remains in the effluent (Pearce et al., 2003). A typical example of such a dye is RR-198 used by the Cameroon Textile Industry (CICAM).

Advanced oxidation processes (AOPs) have over the years proven to be efficient as far as the elimination of textile dyes from solution is concerned. However, most of them often require sophisticated instrumentation and expensive chemical reagents. Nonetheless, the Fenton

reaction is an AOP that uses *OH radicals generated by the reaction in solution between iron (II) ions and hydrogen peroxide to mineralize organic compounds (Fenton, 1984). This process is called the classical or homogeneous Fenton process. The optimal value for the mineralization of organic compounds in solution by the homogeneous Fenton process lies in the range 2 and 4 and this critically limits the efficiency of the process. (Jung et al., 2009). To by-pass this problem, iron has been sustained within the structure of various solid materials serving as catalytic supports. These iron-bearing solid materials can efficiently stimulate the degradation of recalcitrant materials without the formation of ferric hydroxide sludge. This is known as the heterogeneous Fenton process. Many solid materials have been used as heterogeneous catalytic supports for iron in Fenton degradation: iron oxides (Fernandez et al., 2010), high specific surface materials like zeolites (Navalon et al., 2010), graphene oxide sheets (Wang et al., 2019) and clays (Herney-Ramirez et al., 2010), commercial activated carbon samples (Plakas & Karabelas, 2016). However, most of these materials are not readily available and their synthesis requires the use of long procedures, sophisticated equipment and extra chemical reagents.

Biochars are eco-friendly porous materials with large specific surface areas and rich mineral elements (Enders et al., 2012). They have become highly sought after owing not only to their interesting properties but more because of their easy and low-cost route of production. Compared to activated carbons, biochars are produced by the simple pyrolysis of biomass (Tong et al., 2011; Rubeena et al., 2018). The use of biochars as adsorbents for dye removal has been investigated (Jiang et al., 2012; Chen et al., 2011; Liu et al., 2015) but their application as heterogeneous catalytic supports for the Fenton process has received very little attention (Rubeena et al., 2018). Biochar materials cannot by themselves initiate the production of radical species such as *OH radicals given their poor iron content. Reason why they must be subjected to modification with iron salts via an appropriate synthesis procedure. On the other hand, iron bearing materials such as oxides, magnetic graphene particles, magnetic activated carbons and iron-bearing zeolites can efficiently stimulate the degradation of organic pollutants in solution but unlike biochars, the methods of obtaining them are generally longer, require sophisticated apparatus and sometimes extra reagents. This adds to operational cost. Therefore, using iron-bearing biochars leads lower cost, easily affordable eco-friendly and sustainable materials for the same or improved efficiency.

The hydrothermal and co-precipitation methods make use of iron (II) and iron (III) salts as precursors for magnetite production in the reaction medium. It has been demonstrated that these methods are efficient and cost effective for the synthesis of magnetite-based composite materials (Bopda et al., 2022; Ngankam et al., 2020). They are easy to implement, consume less energy due to the fact they do not require extremely high temperatures and necessitate the use of inexpensive chemical reagents. Given their numerous advantages, these methods are of choice in this work for the modification of biochar obtained from orange peels. However, a comparative study of the efficiency of these two methods for synthesizing magnetite and magnetite-based composite materials has not been reported in literature.

It is estimated that over 20 tons of oranges are produced each year in Cameroon and this amount is expected to triple by 2025 (MINADER report, 2015). Half of this amount is exported to foreign countries and the other half is locally consumed generating large quantities of biomass in the form of peels considered as waste. This waste generally ends up in refuse sites where it is partially incinerated alongside other waste products releasing toxic gases into the atmosphere and contributing to global warming. Instead of doing this, the orange peels can be collected, pre-treated by washing and drying, then pyrolyzed to yield biochar. By so doing, the problem of solid waste littering on the streets as well the release of toxic and greenhouse gases can be reduced. Several studies have developed biochars from orange peels and have shown that the surface properties, porosity, and adsorption capacities depend on the preparation conditions (Abdelaal et al., 2021; Abdelhafez and Li, 2016;

Adeniyi et al., 2023, 2020; Amin et al., 2019; Chen and Chen, 2009; Ying et al., 2020; Zhang et al., 2022). In addition, very few works (Ai et al., 2020; Mahmoud et al., 2022; Meng et al., 2017) have developed magnetic biochar from orange peels and no study to our knowledge has used this magnetized biochars as heterogeneous catalytic supports for iron in Fenton degradation of RR-198.

As such, the purpose of this study is to valorize orange peels in view of obtaining magnetite-biochar composite materials for use in the removal of reactive red-198 from solution by the Fenton process. Herein, the response surface methodology is used to evaluate the effect of five parameters (solution pH, composite material dosage, time of stirring, H_2O_2 concentration and initial dye concentration) on the dye removal efficiency.

2. Materials and methods

2.1. Chemicals

Apart from the RR-198 dye of commercial grade obtained from CICAM, all other reagents used in this work are of analytical grade and were used as purchased. 50 %V/V (16.3 mol/L) H_2O_2 was purchased from GFS Chemicals, USA; methanol of purity 99.5 %, NaOH of purity 99 % and HCl of purity 36 % were obtained from BDH Chemicals, Belgium; H_2SO_4 of purity 98 % was obtained from Fisons Scientific, England; $FeSO_4.7H_2O$ and $FeCl_3.6H_2O$ were obtained from Guangdong Guanghua Sci-Tech Co., Ltd China. KCl of purity 99.5 % and $K_3[Fe(CN)_6]$ of purity 98 % were both obtained from Sigma Aldrich, Germany.

2.2. Preparation of biochar

Orange peels were collected from dust bins of the Dschang municipality fruit market in the West region of Cameroon. They were washed thoroughly with distilled water to get rid of earthy impurities and oven dried at 110 °C for 10 h to remove moisture. 500 g of the peels were then placed in an aluminium dish, sealed, and kept in an ISUNU muffle furnace for pyrolysis at 450 °C for 2 h under inert nitrogen atmosphere. The product obtained was ground in a porcelain mortar and sieved to obtain particles of sizes less than 100 μm. This material was coded BC.

2.3. Synthesis of magnetite-biochar composite materials

Hydrothermal synthesis was done using $FeSO_4·7H_2O$ as iron precursor and NaOH. To achieve this, 20 g of $FeSO_4·7H_2O$ was introduced into a 500 mL-conical flask placed on a magnetic stirrer and dissolved using 200 mL of distilled water. 20 g of BC was added to the solution. The temperature of the magnetic stirrer was set at 80 °C and agitation turned on. To the mixture was added 50 mL of NaOH solution of concentration 1 mol/L in a dropwise manner. The mixture was stirred for 1 h and its colour gradually changed from green to black, after which agitation was stopped and the mixture allowed to cool to room temperature. The black residue formed in the course of agitation settled at the bottom of the conical flask and was recovered from a solution by magnetic separation with the help of the bar magnet used in stirring. This residue was washed with distilled water to get rid of any unreacted reagents and oven dried at 110 °C for 4 h. The resulting material was coded Fe_3O_4-BC1 and stored in a desiccator for further use.

Chemical co-precipitation synthesis was done using $FeSO_4·7H_2O$ and $FeCl_3·6H_2O$ as iron precursors and NaOH. 6.6 g of $FeSO_4·7H_2O$ and 13.3 g of $FeCl_3·6H_2O$ were introduced into a 500 mL-conical flask placed on a magnetic stirrer and dissolved using 200 mL of distilled water. 20 g of BC was added to the solution. The temperature of the magnetic stirrer was set at 80 °C and agitation turned on. 50 mL of NaOH solution of concentration 1 mol/L was added dropwise to the mixture in the conical flask. The mixture was stirred for 1 h and its colour gradually changed from reddish-brown to black, after which agitation was stopped and the mixture allowed to cool to room temperature. The black residue formed

during agitation settled at the bottom of the conical flask and was recovered from a solution by magnetic separation with the help of the bar magnet used in stirring. This residue was washed with distilled water to get rid of any unreacted reagents and oven dried at 110 °C for 4 h. The resulting material was coded Fe$_3$O$_4$-BC2 and stored in a desiccator for further use. Pure magnetite particles were also obtained via chemical co-precipitation without the addition of biochar into the reaction mixture.

Magnetite particles are produced in the course synthesis and incorporated within the carbonaceous matrix of the biochar material to afford the magnetite-biochar composite materials. Fig. 1 illustrates the pathway for obtaining the two composite materials from dried orange peels.

2.4. Characterization

The textural and morpho-structural properties of the two composite materials and their biochar precursor were studied using Fourier-transform infrared (FT-IR) spectroscopy, Raman spectroscopy, X-ray diffraction (XRD), scanning electron microscopy (SEM) and energy dispersive spectroscopy (EDX). XRD for crystalline and/or amorphous phase determination was performed using a PAN analytical XPERT Pro powder diffractometer, automated with anode filtered Cu-K$_{\alpha 1}$ radiation. Scanning of the samples was done under conditions of radiation wavelength (λ) = 1.54056 \AA, accelerating voltage of 45 kV at 40 mA, a 2θ range between 10 and 90° and a time constant of 27.5400 s with step interval (2θ/step) of 0.0260. Functional groups present in the materials were investigated by FT-IR spectroscopy in attenuated total reflection mode using a Nicolet Thermoscientific IS5 spectrophotometer. The spectra were recorded in the range of 4000 to 500 cm^{-1}. SEM and EDX analyses were done TESCAN VEGA 3-LMU AT 8 kV. The samples were mounted on aluminium stubs and coated with thin films of gold sputter to make them conductive prior to analysis. The Raman spectra of the three materials were recorded with a Raman spectrometer Almega X Thermo using laser excitation line at 532 nm. A beam of monochromatic light produced by a continuous laser is focused on the sample to be analysed, the photons are in small part diffused with a change in frequency. The change in frequency is detected as inelastic scattering or Raman scattering. The specific surface area, pore size and pore volume of the three materials were determined from N$_2$ adsorption and desorption using the BET/BJH models. A BELSORP MAX apparatus from Bel Japan Inc was used for this purpose. The sorption experiments were carried out at 77 K. Electrochemical impedance spectroscopic (EIS) measurements were performed using a carbon paste electrode in a solution of 5 mmol/L [Fe(CN)$_6$]$^{3-/4-}$ as electrolyte in 0.1 mol/L KCl. A frequency range of 1 MH to 0.1 Hz at a potential of 0.25 V was used for this purpose.

2.5. Heterogeneous Fenton degradation experiments

The degradation experiments were carried out in batch mode at ambient temperature in the presence of daylight. For each run, 50 mL of the pollutant solution adjusted to the required concentration and pH were put into a conical flask, followed by the addition of 5 mL of H$_2$O$_2$ of the required concentration and a given mass of the magnetite-biochar composite material. The mixture was stirred for the required time using a magnetic stirrer and after the time of stirring, a 5 mL aliquot was withdrawn with a pipette and filtered using Whatman filter paper number 3. Two drops of methanol were immediately added to the filtrate to quench the radical reaction (Wang et al., 2019). The absorbance of the filtrate was then read off from a UV–visible spectrophotometer (UV Genesys 10S UV–visible spectrophotometer, Thermo Scientific) at λ_{max} of 520 nm to determine the dye equilibrium concentration. The percentage degradation (%R) of the reactive-198 dye was then calculated using Eq. (1).

$$\%R = \frac{C_o - C_t}{C_o} \times 100 \qquad (1)$$

where C$_o$ and C$_t$ are the concentrations (mg/L) of the dye solution before and after each degradation experiment respectively.
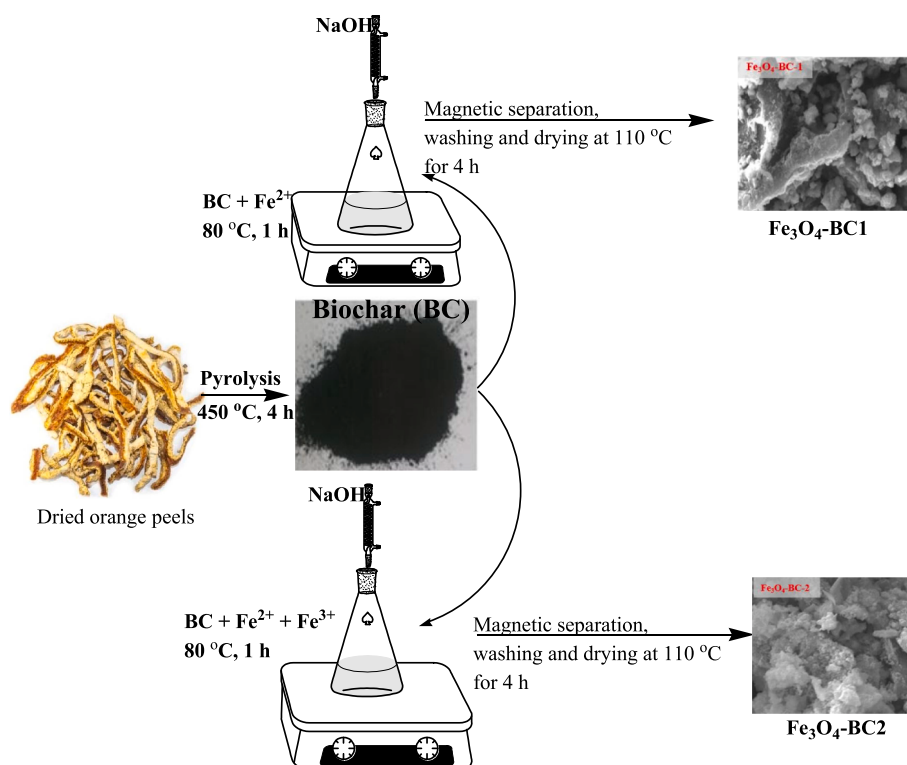
Fig. 1. Synthesis procedure of composite materials from dried orange peels.

2.6. Central composite design (CCD) of the Fenton degradation experiments

The response surface methodology of the CCD was used to optimize the operation parameters of the dye degradation. To simultaneously study the effects of the interaction among three or more factors on the outcome of a given process, the CCD is highly recommended to reduce the number of error attempts (Bezerra et al., 2008; Makela, 2017). In this work, the effect of five parameters were investigated simultaneously: solution pH (A), between 2 and 8; RR-198 concentration (B), between 25 and 100 mg/L; H_2O_2 concentration (C) between 4.1 and 16.3 mol/L; mass of composite material (D) between 100 and 300 mg and time of stirring (E) between 15 and 45 min (Table 1). The highest value for each parameter was coded +1, the lowest value coded as −1 and the value at the centre coded as 0. The centre value is obtained by dividing the sum of the highest and lowest values by 2. For five independent variables and four centre points, the CCD generates 46 experiments according to Eq. (2).

$$N = 2^k + 2k + n = 2^5 + 2(5) + 4 = 46 \qquad (2)$$

where, N is the total number of experiments to be run, k is the number of experimental variables and n is the number of centre points chosen. The number of points at the centre is critical for determining experimental errors and evaluating the reproducibility of results obtained.

To minimize the effects of uncontrolled parameters, the 46 experiments were randomly carried out in one block. The Statgraphics Plus version 5.0 software was used to design the experiments. For each experiment, the expected response, Y was the percentage degradation (R) of the dye. An empirical model was developed based on the response of each of the 46 experiments. The interactions between the experimental parameters and their influence on the expected response are fitted into the classical second-order polynomial equation with its linear terms as given by Eq. (3). This equation shows the empirical mathematical model used to evaluate the correlation between the responses obtained experimentally and those predicted by the software.

$$R = \beta_0 + \sum_{i=1}^{n} \beta_i x_i + \sum_{i=1}^{n} \beta_{ii} x_i^2 + \sum_{i=1}^{n} \sum_{j=1}^{n} \beta_{ij} x_i x_j + \varepsilon \qquad (3)$$

R is the predicted response, β_0 is the constant of the quadratic equation, β_i is the linear coefficient, β_{ii} is the quadratic coefficient, β_{ij} is the coefficient of the interaction between the variables, x_i and x_j are the coded values of the parameters studied in the degradation experiments and ε is the uncertainty between measured and predicted values.

2.7. Analysis of variance (ANOVA) and validation of the statistical model

The STATGRAPHIC Plus 18.0 software was used to evaluate the statistical analysis of the experimental data and to validate the statistical model describing the Fenton degradation experiments. The software uses four criteria for this evaluation: (1) each factor must present a p-value, that is, the value of the probability smaller than 5 % within a confidence limit of 95 %, (2) the value of regression coefficients, R^2 must be as close as possible to 1, indicating that the experimental values and

the predicted values of the response are close to each other, (3) the t-test must be significant (p < 0.05), showing that the model adequately describes the experimental data, and finally (4) the closeness between the data of the predicted points and the data of the experimental points must present a normal distribution for the hypothesis made by the analysis of variance (ANOVA) to be validated.

2.8. Kinetic studies of the Fenton degradation reactions

The first and second order kinetic rate laws were used to investigate the kinetics of the degradation reaction of RR-198 in solution. For simplicity, it is assumed that the rate of the oxidation reactions of organic molecules in solution in the presence of *OH radicals depends on the concentration of the organic molecule alone given that the concentration of *OH radicals in solution remains fairly constant (Mafo et al., 2023). Eqs. (4) and (5) respectively give the linear forms of the first and second order kinetic rate laws.

$$-\frac{dC}{dt} = kc \Rightarrow \ln\frac{C_0}{C_t} = kt \qquad (4)$$

$$-\frac{dC}{dt} = kc^2 \Rightarrow \frac{1}{C_t} - \frac{1}{C_0} = kt \qquad (5)$$

where t is the time of degradation; C_t is the concentration of the RR-198 dye after time of degradation, t; C_o is the initial concentration of the dye at time t = 0, and k is the rate constant.

From linear plots of $\ln(C_o/C_t)$ and $1/C_t = f(t)$, the first and second order rate constants and half-lives of the degradation reaction were determined.

2.9. Magnetic recovery and reuse of the composite materials

The reusability of the two synthesized composite materials was studied by first recovering them from solution using a bar magnet after every degradation experiment under optimum conditions provided by the CCD. The recovered materials were oven-dried before reuse in another degradation experiment. Their catalytic activity was evaluated over four cycles of degradation of the dye and the results obtained over these cycles compared.

Table 1
Experimental variables for the CCD of the degradation experiments.

Parameter	Units	Coded variables	Variables levels		
			−1	0	+1
pH	/	A	2.0	5.0	8.0
[RR-198]	mg/L	B	25.0	62.5	100.0
[H_2O_2]	mol/L	C	4.1	10.2	16.3
Mass of composite	Mg	D	100	200.0	300.0
Time of stirring	Min	E	15.0	30.0	45.0
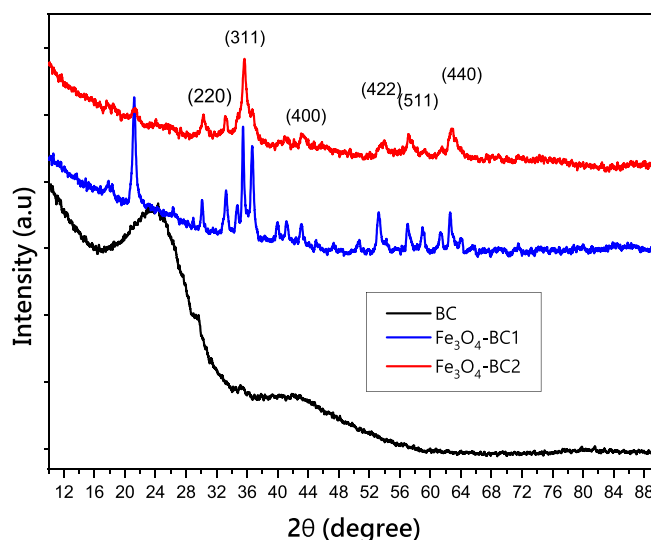
Fig. 2. XRD patterns of BC, Fe_3O_4-BC1 and Fe_3O_4-BC2.

3. Results and discussion

3.1. Characterization of BC, Fe_3O_4-BC1 and Fe_3O_4-BC2

The XRD pattern of BC in Fig. 2 shows the absence of peaks, indicating that biochar produced from lignocellulosic biomass such as orange peels is an amorphous material (Armynah et al., 2018). On the other hand, the diffraction patterns of Fe_3O_4-BC1 and Fe_3O_4-BC2 have characteristic crystalline peaks occurring at 2θ values of 30.2, 35.5, 43.3, 53.7, 57.2 and 62.1°. These peaks correspond to the miller indices of (2 2 0), (3 1 1), (4 0 0), (4 2 2), (5 1 1) and (4 4 0) respectively, and are indicative of the inverse cubic spinel group of magnetite. Similar results have been reported in literature for the synthesis of pure magnetite particles (Chaki et al., 2015), and magnetite based composite materials (Gareth & James, 2021). This result shows that both the hydrothermal and co-precipitation methods can successfully lead to the impregnation of magnetite particles into the matrices of lignocellulosic biomass materials such as orange peels. However, it can also be observed that other peaks not belonging to magnetite occur at $2\theta = 21.1$, 34.9, 41.4 and 59.3 on the diffraction patterns of the two composite materials. The extra peaks at $2\theta = 21.1$, 34.9, 41.4 and 59.3 common to both composite materials are evidence of another iron oxide or hydroxide phase formed during synthesis by both methods. These peaks correspond to the crystalline phase of goethite (FeO(OH)), which is a by-product formed alongside magnetite during the synthesis reaction (Khelifi et al., 2016).

The superposed FT-IR spectra of BC, Fe_3O_4-BC1 and Fe_3O_4-BC2 are presented in Fig. 3 and confirm the presence of magnetite in the composite materials by the existence of a very intense band around 550–570 cm^{-1} that corresponds to the symmetric stretching vibrations of O—Fe—O bonds in magnetite. Worthy of attention is the occurrence of two bands on the spectra of Fe_3O_4-BC1 and Fe_3O_4-BC2 around 800 and 900 cm^{-1}, characteristic of the O—H bending vibrations of the Fe—OH group in goethite and are respectively on behalf of the vibrations in and out of the plane (Khelifi et al., 2016). These results agree with the XRD results presented and discussed above. Also interesting is the fact that the O—Fe—O band of magnetite is much more intense than the Fe—OH band of goethite, indicating that magnetite is the dominant iron oxide phase present in the two composite materials. Again, the Fe—OH band of goethite on the spectrum of Fe_3O_4-BC1 is more intense than that on the spectrum of Fe_3O_4-BC2, implying that the co-precipitation method is more efficient in converting iron salt precursors to magnetite than the hydrothermal method. The band around 3100–3300 cm^{-1} is present
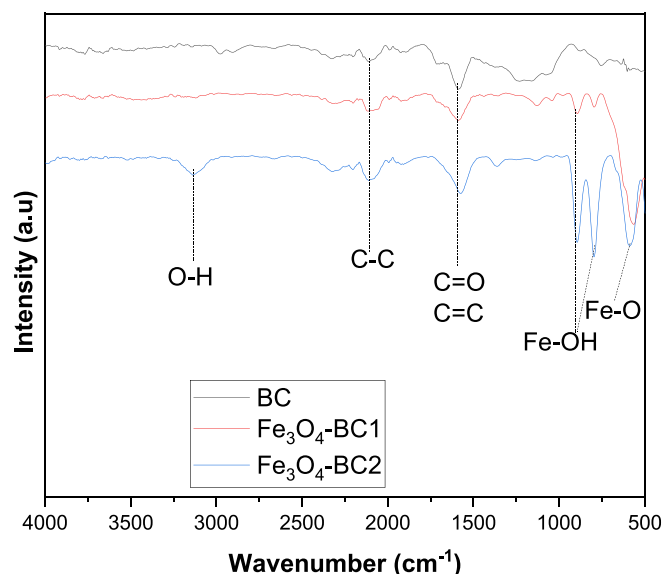
only in Fe_3O_4-BC1 and is probably due to the absorption of moisture by the latter. The spectrum of BC shows no bands between 3000 and 3500 cm^{-1} meaning that pyrolysis led to the complete removal of moisture from the orange peel biomass to afford a carbon-rich residue. The spectra of the three materials show common bands around 1625 cm^{-1} and 2120 cm^{-1}. That around 1625 cm^{-1} can be attributed to elongation vibrations of C=C of the aromatic rings of lignin and to carbonyl and carboxylic acid functions while the other around 2120 cm^{-1} can be assigned to —C—C— aliphatic stretching vibrations. All these bands confirm the co-existence of biochar and magnetite in the same solid phase for the two synthesized composite materials. Similar results have been reported in literature (Bopda et al., 2022; Ngankam et al., 2020).

The Raman spectrum of BC has a band present around 1350 cm^{-1} (Fig. 4). This band is called the D-band and it is typical of the disorder in amorphous structure of carbon-based materials like graphene (Wang et al., 2019), activated carbons and biochar. Another band occurs around 1590 cm^{-1} called the G-band and is attributable to the E_{2g} symmetric vibration mode of the sp^2 hybridized carbon atoms of graphitic carbon (Wang et al., 2019). Information regarding structural defects and degree of disorder in carbon-based materials can be obtained from the ratio of the intensity of these two bands (I_D/I_G) (Mady et al., 2017). This ratio is approximately 1.0 for BC, comparable to the values obtained by Wang et al. (2019), Mady et al. (2017) and Li et al. (2017) for graphene. Such a value confirms the amorphous nature of carbon-based materials and equally suggests that they are of less structural disorder compared to crystalline solids like magnetic iron oxides. This fact is again further confirmed by the absence of bands on the Raman spectra of the two composite materials, evidence of a structural transformation of the amorphous biochar to crystalline solids during synthesis by the impregnation of iron oxides mainly in the form of magnetite into the matrix of the biochar material. This change potentially improves the catalytic properties and hence increase the efficiency of dye removal by the Fenton process. Magnetite is a solid containing a mixture of Fe^{2+} and Fe^{3+}, it can therefore facilitate the formation of *OH radicals from H_2O_2 needed for dye degradation without any leaching of iron hydroxides in the reaction medium compared to the homogeneous Fenton process.

The surface morphology of the two composite materials alongside their biochar precursor is shown in the SEM images in Fig. 5. The SEM image of BC presents a porous surface, this can be explained by the fact that pyrolysis under high temperatures favours the development of pores by the escape of volatile materials such as oxides of carbon and water from the biomass. On the other hand, there is no significant

Fig. 3. FT-IR spectra of BC, Fe_3O_4-BC1 and Fe_3O_4-BC2.
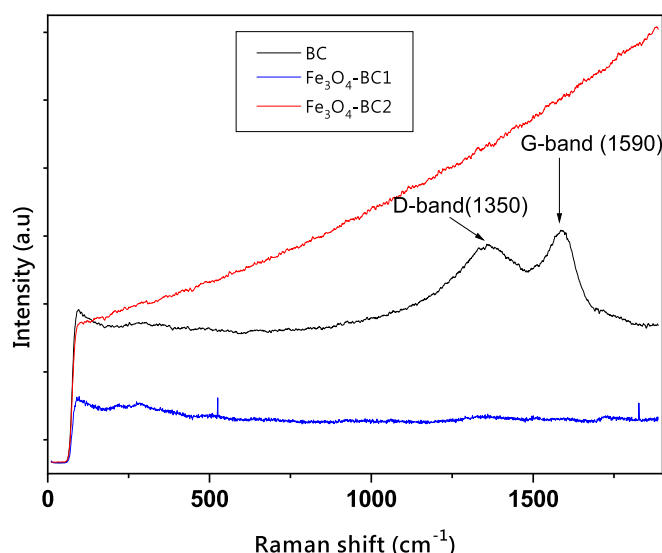
Fig. 4. Raman spectra of BC, Fe_3O_4-BC1 and Fe_3O_4-BC2.
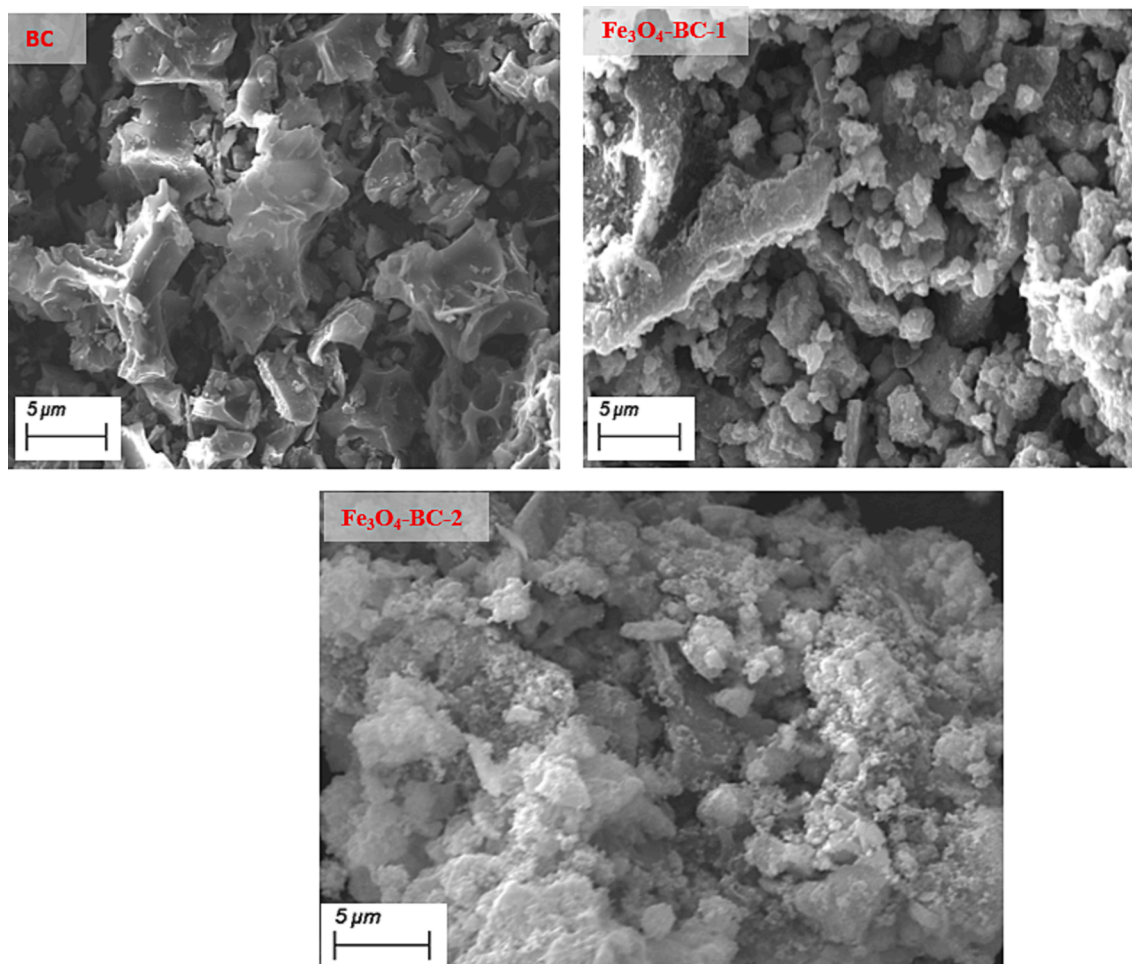
Fig. 5. Scanning electron micrographs of BC, Fe_3O_4-BC1 and Fe_3O_4-BC2.

surface morphological difference between Fe_3O_4-BC1 and Fe_3O_4-BC2: their SEM images present an agglomeration of granulated solid particles. Nonetheless, their SEM images show that unlike BC, the cavities on their surfaces have been filled by iron oxides, mainly magnetite particles. Studies have shown that the development of cavity-shaped pores on the surface of materials during pyrolysis is advantageous if the given material must be subjected to subsequent modification. It is the case with BC given that the pores it develops on its surface during pyrolysis favour the adsorption and impregnation of iron oxide particles onto its carbonaceous and oxygenated surface during modification by the hydrothermal and co-precipitation methods. These results are consistent with those obtained by Peng et al. (2022) and Zhou et al. (2019). This assertion agrees with the EDX mappings of the two composite materials (Figs. 6 and 7) that reveal the presence of magnetite particles incorporated within the carbon matrix of the biochar precursor. These EDX maps also indicate the surface of Fe_3O_4-BC2 is less homogenous than that of Fe_3O_4-BC1. From this assertion, it can be deducted that the co-precipitation method is more successful than the hydrothermal method given that the less homogeneous surface means the magnetite particles are almost indistinguishable from the biochar particles indicating better impregnation of magnetite particles into the matrix of the biochar precursor. This assertion ties with the FT-IR results presented and discussed above.

Elemental composition by EDX analysis of the two composite materials as well as their biochar precursor is represented in Figs. 6, 7 and 8. From these, it can be confirmed that the pyrolysis of the orange peels to afford BC was successful given that it contains only carbon (80.4 %) and oxygen (19.6 %). During pyrolysis, volatile material is lost from the

biomass in the form of H_2O, oxides of carbon, nitrogen, and sulphur to leave a carbon rich residue. The X-ray diffractogram and Raman spectrum of BC corroborate the success of pyrolysis and the carbon-rich residue obtained at the end of pyrolysis. Similar results have been obtained by Chen et al. (2011) and Bopda et al. (2022) to produce biochar from lignocellulosic biomass. In addition to carbon and oxygen, Fe_3O_4-BC1 and Fe_3O_4-BC2 also contain high percentages of iron and small amounts of sodium: 26.6 % C, 42.5 % Fe, 27.2 % O, 3.7 % Na and 51.4 % C, 14.1 % Fe, 33.7 % O, 0.8 % Na, respectively. The small percentages of sodium come from the addition of NaOH solution to the reaction mixture during synthesis by both methods. However, the composition is very small indicating that the materials were properly washed and rinsed with distilled water after synthesis before use. The appearance of iron in high amounts is an indication of the success of both methods of synthesis. XRD patterns and FT-IR spectra confirm that iron in the two composite materials is present in the form of oxides, mainly magnetite.

N_2 adsorption/desorption isotherms for the precursor and the activated carbon are illustrated in Fig. 9(a) and the pore size distribution in Fig. 9(b). As presented in Table 2, BET analyses shows that the specific surface area of BC, Fe_3O_4-BC1 and Fe_3O_4-BC2 are 409.959, 239.142 and 273.306 m^2/g respectively. The adsorption isotherms of all three materials present essentially a type II shape, according to the IUPAC classification, which is typical for non-porous solids (Thommes et al., 2015).

The large specficic surface area of BC once more confirms the success of pyrolysis of the orange peel biomass to produce biochar. This large specific surface are can be atrributed to the loss of volatile matter in the form of oxides of carbon, nitrogen and sulfur as well as moistre form the biomass due to the high temperatures of pyrolysis. Katibibi et al. (2021)
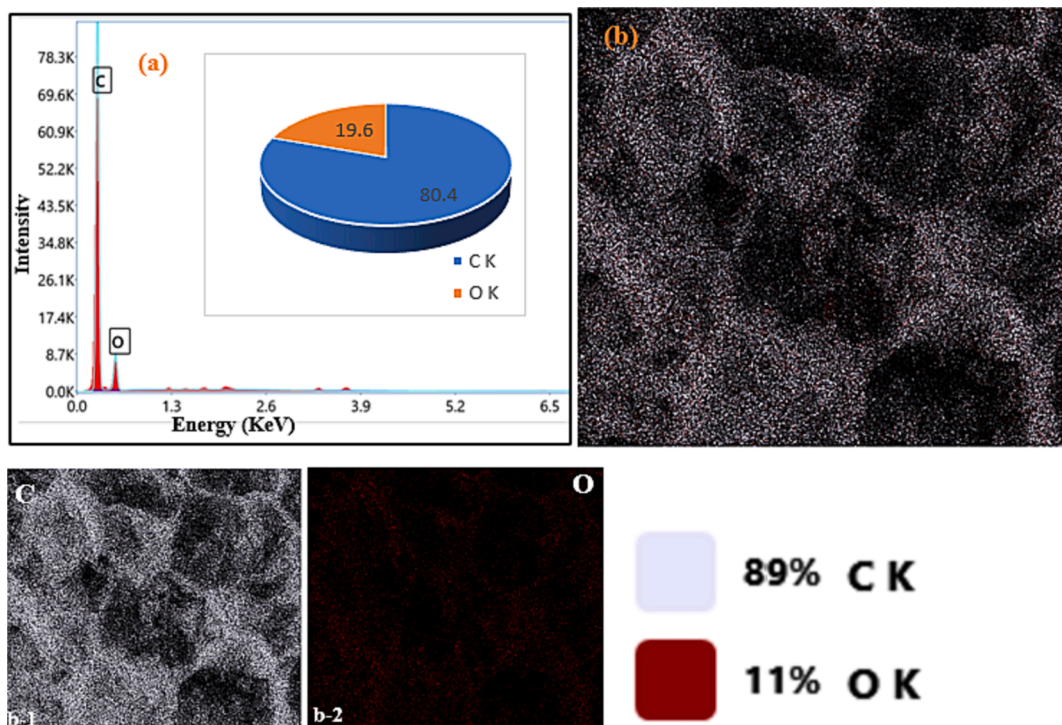
Fig. 6. EDX elemental compositions (a), EDX-mapping (b) and element distribution mapping of C and O, (from b1 to b2 respectively) for the BC.
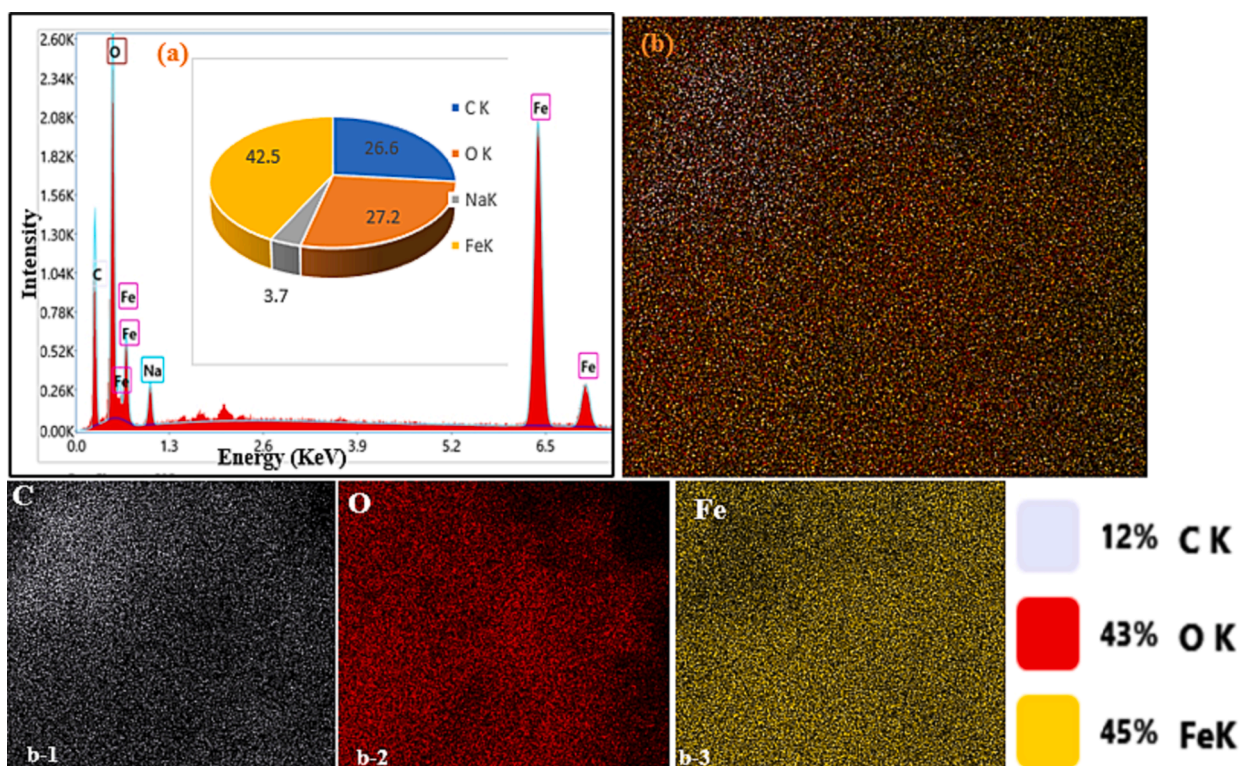
Fig. 7. EDX elemental compositions (a), EDX-mapping (b) and element distribution mapping of C, O and Fe (from b1 to b3 respectively) for the Fe_3O_4-BC1.

obatined S_{BET} of 536.539 m^2/g for biochar obtained from the pyrolysis of palm kernel shells. This higher value is most probably due to the higher temperature of pyrolysis and a longer time of residence of the palm kernel shells in the furnace. On the other hand, the value is much larger than that obtained by Zhang et al. (2022) for biochar obtained from ornage peels pyrolysed at a lower temperature of 400 °C for a shorter resiedence time of 2 h. This shows that increasing the temperature of pyrolysis and the residence time of the biomass in the furnace brings about a biochar prodcut of greater specific surface area and porosity. The specific surface areas of Fe_3O_4-BC1 and Fe_3O_4-BC2 show a considerable decrease that occurs as a result of hydrothermal and co-precipitated modifications of BC. This once more confirms the success
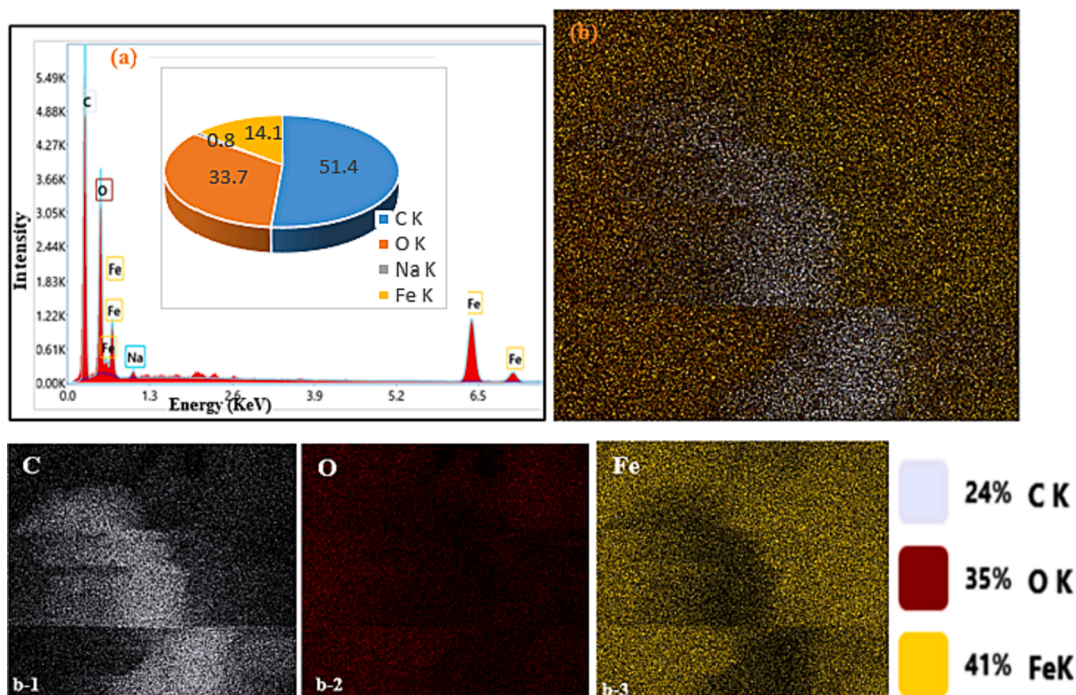
Fig. 8. EDX elemental compositions (a), EDX-mapping (b) and element distribution mapping of C, O and Fe (from b1 to b3 respectively) for the Fe$_3$O$_4$-BC2.
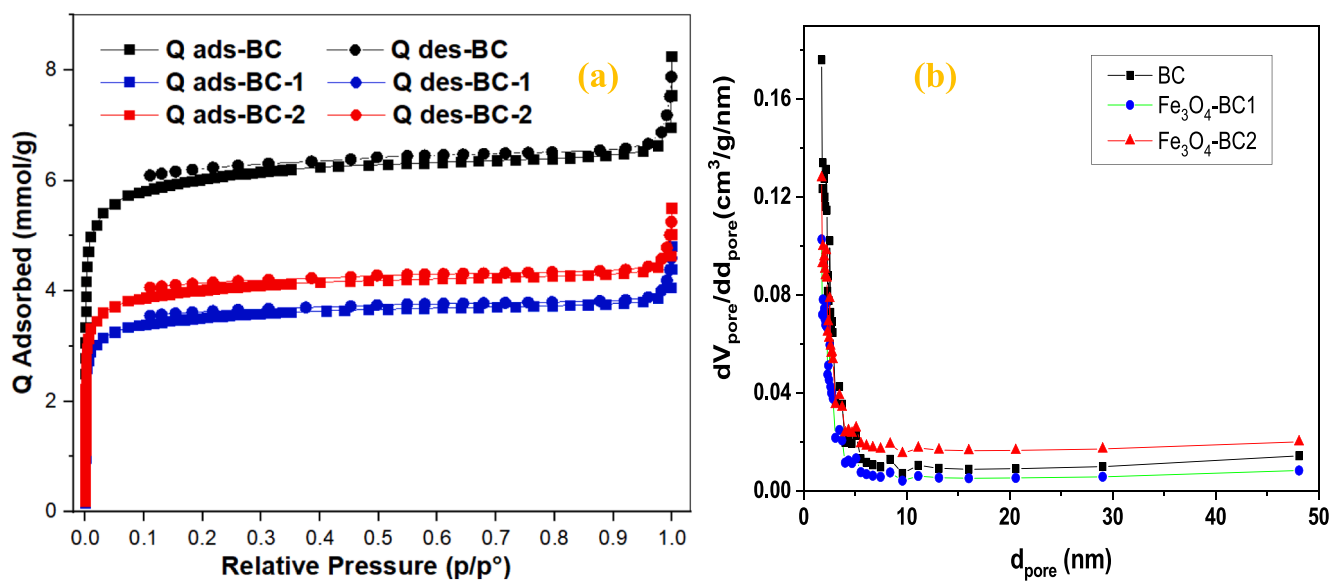
Fig. 9. N$_2$ adsorption–desorption isotherm (a) and BHJ pore size distribution (b) of BC, Fe$_3$O$_4$-BC1 and Fe$_3$O$_4$-BC2.

Table 2
Summary of N$_2$ adsorption-desorption analyses of BC, Fe$_3$O$_4$-BC1 and Fe$_3$O$_4$-BC2.

	BC	Fe$_3$O$_4$-BC1	Fe$_3$O$_4$-BC2
Micropore area (m^2/g)	317.70	185.32	211.80
External surface area (m^2/g)	92.23	53.82	61.51
S$_{BET}$ (cm^2/g)	409.93	239.14	273.31
Mean pore volume (cm^3/g)	0.168	0.098	0.112

of the impregantion of iron-oxide particles in the form of magetite onto the carbonacoes matrix of BC. This percitible dercrase in the specific surcae area and porosity from the biochar precursor to the iron-modified composites can be expalined by the fact that magnetite particles clog some of the active sorption sites of BC during modification, thereby corroborating the SEM-EDX results presented and discussed above. In a similar manner, the mean pore diameter, area and volume of BC are much higher than those of Fe$_3$O$_4$-BC1 and Fe$_3$O$_4$-BC2 for the same reason. Survey of literature reveals similar results for iron-modified carbonaceous materials obatined from pyrolysed lignocellusosic biomass (Katibi et al., 2021).

The Nyquist plots obatined from EIS measurements (Fig. 10.) with reference to the standard carbon paste electrode (CPE) show that conductivy decresaes in the order Fe$_3$O$_4$-BC2 > Fe$_3$O$_4$-BC1 > BC. This means the iron oxide particles incorpotared within the carbonacoes matrix of the precursor material during hydrothermal and co-precipitation modifcation reactions greatly incerase the condicutivity of the materials. Also, it can be seen that the composite material
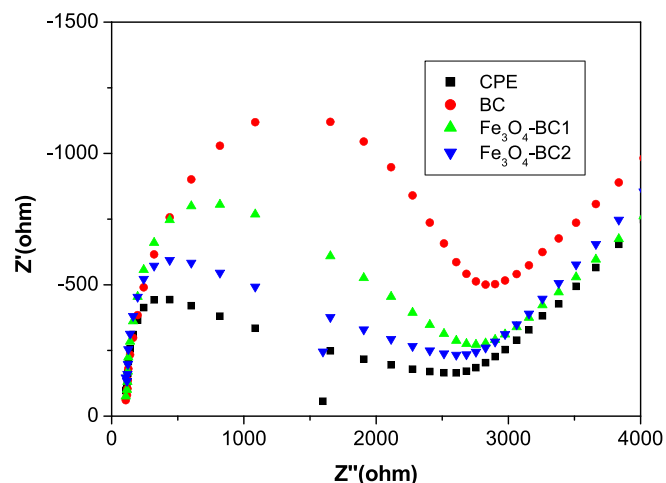
obtained by co-precipitation has a lower chrage transfer resistance compatred to that obatined by hydrothermal synthesis. For reactions in solution such as the Fenton process that are greatly influenced by the formation of radical species, low charge transfer resistance is of utmost importance as it determines the rate of formation of *OH by the action of H$_2$O$_2$ on the surface of the material containing iron species.

3.2. Comparing the efficiency of RR-198 removal based on different systems

The removal of RR-198 was evaluated in the presence of the biochar material (BC), the composite biochar materials (Fe$_3$O$_4$-BC1 and Fe$_3$O$_4$-BC2) as well pure magnetite particles without the addition of H$_2$O$_2$ in the reaction medium. The results obtained from these tests are presented in Fig. 11. Dehghani et al. (2018) reported an adsorptive removal efficiency of 88 % for RR-198 after 30 min of contact with pure magnetite particles obtained via co-precipitation. The value obtained in this work is far less compared to their theirs. BC demonstrates higher adsorptive capabilities as over 73 % of the dye can be eliminated after 45 min of contact with it compared to the three other materials. This can be
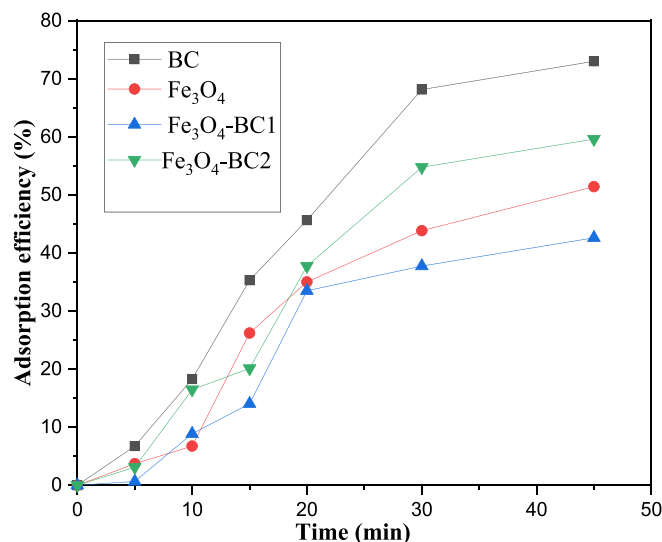
attributed to its higher SBET of 409.93 m^2/g. The much lower adsorption capacities observed with the composite biochar materials (42.62 and 59.65 respectively for Fe$_3$O$_4$-BC1 and Fe$_3$O$_4$-BC2) are most probably due to the fact that the porous surface of the biochar has been cover by the impregnation of iron-oxide particles in the course of modification. The pure magnetite particles show moderate adsorptive capability for the dye after 45 min (51.44 % removal).

In addition, the efficiency of dye removal based on different heterogeneous Fenton systems (Fig. 12) was evaluated in order to determine the materials to be used for the experimental design. The modified composite biochars show superior degradation efficiency after 45 min of stirring (91.88 % and 96.14 % respectively for Fe$_3$O$_4$-BC1 and Fe$_3$O$_4$-BC2) over pure magnetite particles (73.03 %). Based on these results, the design of the degradation experiments was performed considering the two magnetite-biochar composite materials.

3.3. Experimental design of degradation experiments and statistical validation of the postulated model

R$_1$ and R$_2$ are the amounts of RR-198 in percentage degraded in solution in the presence of Fe$_3$O$_4$-BC1 and Fe$_3$O$_4$-BC2, respectively. Table 4 presents the experimental design matrix for the degradation of RR-198 in the presence of Fe$_3$O$_4$-BC1 and Fe$_3$O$_4$-BC2 and the results obtained by experiment alongside those predicted by the Statgraphics 18 and sigmaPlot 14.0 software for each run. Eqs. (6) and (7) are the quadratic model equations representing the fit between the predicted response and the five coded variables: pH of the solution (A), concentration of RR-198 (B), concentration of H$_2$O$_2$ (C), mass of composite material (D) and time of stirring (E). The residue values in Table 3 are much lower than the experimental and theoretical values. It can therefore be inferred that the experimental and theoretical values are close to each other, meaning there is a good correlation between them. Therefore, to assess the quality of the two models, the coefficients of determination and adjusted coefficients of determination were evaluated. They are 90.56 and 83.01 % for R1; 96.46 and 93.62 % for R2. The value recommended in several studies to judge the quality of the model is 80 % for the adjusted coefficient of determination. The values obtained are in good agreement with this recommendation. These results are confirmed by the relationship between the experimental and predicted values of R$_1$ and R$_2$ (Fig. 13), showing good proximity between the values predicted by the model and those obtained experimentally.

Fig. 11. Adsorptive removal of RR-198 in the presence of various materials (mass of material = 300 mg, time of stirring = 45 min, solution pH = 2.00, [RR-198] = 25 mg/L).
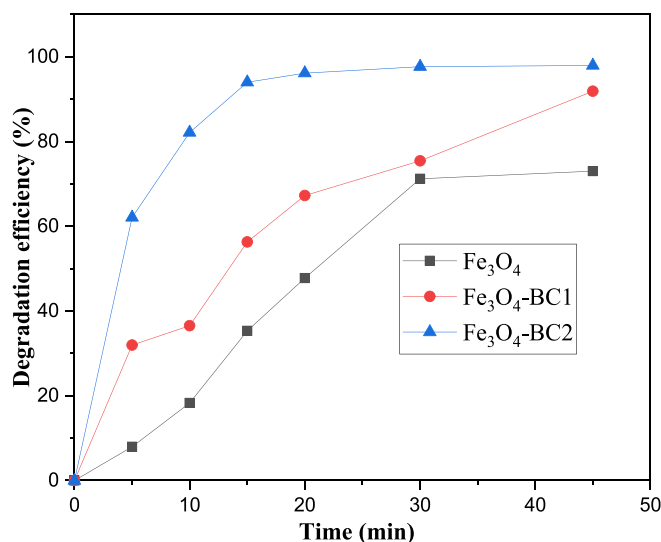
Fig. 12. Removal of RR-198 by Fenton degradation using Fe$_3$O$_4$, Fe$_3$O$_4$-BC1 and Fe$_3$O$_4$-BC2 as catalytic supports (mass of material = 300 mg, [RR-195] = 25 mg/L, [H$_2$O$_2$] = 10 mol/L, time off stirring = 45 min, solution pH = 2).

Table 3

Experimental design matrix showing experimental and predicted responses for the degradation of RR-198 alongside the residues for each experimental run.

No	Factor					Response: percentage degradation, R (%)					
	A	B	C	D (mg)	E (min)	R_1		Rsd	R_2		Rsd
		(mg/L)	(mol/L)			Exp	Pdt		Exp	Pdt	
1	8	25	16.3	100	15	16.01	16.23	0.22	9.52	11.86	2.34
2	5	100	10.2	200	30	13.70	6.80	6.9	52.39	53.95	1.56
3	5	62.5	10.2	200	45	35.02	33.85	1.17	62.17	61.71	0.46
4	8	25	4.1	300	15	5.56	12.10	6.54	9.54	11.86	2.32
5	5	25	10.2	200	30	12.52	26.08	13.56	54.63	53.90	0.73
6	8	25	16.3	300	15	9.40	3.04	6.36	34.05	33.44	0.61
7	5	62.5	4.1	200	30	10.33	12.93	2.6	36.78	33.41	3.37
8	8	62.5	10.2	200	30	3.05	17.51	14.46	38.55	39.16	0.61
9	5	62.5	10.2	200	30	29.06	20.79	8.27	45.14	45.73	0.59
10	2	100	16.3	100	45	45.58	29.42	16.16	69.94	70.05	0.11
11	8	100	4.1	300	45	11.55	13.93	2.38	63.68	61.77	1.91
12	8	100	16.3	300	45	8.55	1.80	6.75	22.45	34.07	11.62
13	8	25	4.1	100	45	6.68	2.04	4.64	57.4	51.19	6.21
14	2	25	4.1	300	15	93.11	90.92	2.19	77.46	74.86	2.6
15	2	25	4.1	100	45	93.11	90.92	2.19	75.36	83.55	8.19
16	5	62.5	16.3	200	30	69.13	65.66	3.47	14.04	18.24	4.2
17	8	100	16.3	100	15	4.68	8.74	4.06	15.68	15.13	0.55
18	8	100	4.1	300	15	8.26	18.53	10.27	63.28	62.81	0.47
19	5	62.5	10.2	100	30	9.95	9.78	0.17	31.53	36.41	4.88
20	2	25	16.3	100	45	72.3	74.40	2.1	75.36	73.05	2.31
21	2	100	4.1	300	45	59.2	51.62	7.58	77.03	76.13	0.9
22	2	100	16.3	100	15	33.78	27.68	6.1	68.06	70.01	1.95
23	2	25	4.1	100	15	66.86	68.49	1.63	71.44	68.30	3.14
24	8	25	4.1	300	45	8.56	7.93	0.63	65.05	66.03	0.98
25	5	62.5	10.2	200	15	27.24	35.07	7.83	57.24	58.53	1.29
26	2	100	16.3	300	45	10.53	28.27	17.74	72.41	68.02	4.39
27	5	62.5	10.2	300	30	7.80	14.63	6.83	52.26	48.21	4.05
28	2	100	4.1	100	45	15.59	28.74	13.15	74.82	74.12	0.7
29	5	62.5	10.2	200	30	29.24	20.79	8.45	49.98	45.73	4.25
30	8	25	16.3	100	45	13.57	21.99	8.42	18.02	21.11	3.09
31	8	25	4.1	100	15	10.47	1.26	9.21	34.73	34.09	0.64
32	2	25	16.3	300	15	70.2	70.63	0.43	65.01	68.17	3.16
33	2	100	16.3	300	15	20.69	31.47	10.78	75.37	78.76	3.39
34	2	25	16.3	300	45	73.03	67.85	5.18	65.53	64.79	0.74
35	2	25	4.1	300	45	77.59	83.15	5.56	78.25	79.35	1.1
36	2	100	4.1	100	15	17.40	31.98	14.58	69.50	66.25	3.25
37	2	25	16.3	100	15	72.30	72.23	0.07	68.82	65.65	3.17
38	5	62.5	10.2	200	30	22.70	20.79	1.91	41.94	45.73	3.79
39	2	62.5	10.2	200	30	72.16	64.36	7.8	73.03	73.24	0.21
40	8	100	4.1	100	45	6.46	2.64	3.82	39.09	40.69	1.6
41	8	100	4.1	100	15	10.05	2.29	7.76	27.33	30.95	3.62
42	8	100	16.3	300	15	9.15	1.41	7.74	51.98	42.96	9.02
43	8	25	16.3	300	45	10.54	3.85	6.69	35.19	31.92	3.27
44	2	100	4.1	300	15	77.20	59.81	17.39	75.9	79.03	3.13
45	8	100	16.3	100	45	7.80	14.55	6.75	22.79	17.02	5.77
46	5	62.5	10.2	200	30	28.79	20.79	8	49.17	45.73	3.44

Exp = Experimental value, Pdt = predicted value, Rsd = Residue (|Pdt - Exp|).

$$R_1 = 117.036 - 35.6351A - 0.264B + 6.456C + 0.519D - 3.748E$$
$$+ 2.239A^2 + 0.083AB + 0.153AC - 0.009AD + 0.019AE - 0.003B^2$$
$$- 0.009BC + 0.001BD - 0.001BE - 0.267C^2 - 0.009CD + 0.0144CE$$
$$- 0.001D^2 - 0.001DE + 0.061E^2$$

(6)

$$R_2 = 97.741 - 17.937A - 0.772B + 11.543C + 0.161D - 3.001E + 1.164A^2$$
$$- 0.002AB - 0.268AC + 0.0159AD + 0.011AE + 0.006B^2$$
$$+ 0.007BC + 0.001BD - 0.003BE - 0.535C^2 - 0.002CD$$
$$- 0.021CE - 0.001D^2 - 0.002DE + 0.064E^2$$

(7)

3.4. Analysis of variance of the postulated model

The significance of the various terms appearing in the two postulated models for the degradation by the Fenton process of RR-198 in the presence of Fe$_3$O$_4$-BC1 and Fe$_3$O$_4$-BC2 were evaluated by the analysis of the variance of the 2 models obtained. The Table 4 presents the results of this analysis. For the R_1 model, 5 factors have p-values less than 0.05 while for the R_2 model, 12 factors have p-values less than 0.05. Therefore, at 95 % confidence, 5 factors are significant for R_1, namely, 2 interactions (AB and CD), one quadratic effect (A^2) and two main factor effects (A and B). As for R^2, 12 factors are significant, namely 3 main effects of the factors (A, C, D), 4 interactions between the factors AC, AD, DE and DE and four quadratic effects of the factors (A^2, B^2, C^2, and E^2). Whatever the Fenton process used for the degradation of RR-198 in this study, it appears that the pH is the only factor whose simple and quadratic effects are significant for the 2 models. In addition, pH is involved in many significant interactions for both models, thus showing its importance for the degradation of RR-198 by a Fenton process in the presence of Fe$_3$O$_4$-BC1 and Fe$_3$O$_4$-BC2. These results are in line with the works of several authors (Kremer, 2003; Lu et al., 2018; Wypych, 2018) who have demonstrated the strong dependence of the Fenton reaction on the pH of the medium.

Table 4
Analysis of variance for the degradation of RR-198 in the presence of Fe_3O_4-BC1 and Fe_3O_4-BC2.

Factor (or interaction)	Fe_3O_4-BC1				Fe_3O_4-BC2			
	Df	MS	ƒ ratio	P value	Df	MS	ƒ ratio	p value
A	1	18651.2	152.32	**0.0000**	1	9872.64	384.05	**0.0000**
B	1	3158.06	25.79	**0.0000**	1	0.0165	0.00	0.9800
C	1	149.227	1.22	0.2801	1	1957.31	76.14	**0.0000**
D	1	199.36	1.63	0.2137	1	1183.54	46.04	**0.0000**
E	1	12.554	0.10	0.7515	1	85.892	3.34	0.0795
AA	1	1000.96	8.17	**0.0084**	1	270.573	10.53	**0.0033**
AB	1	2817.0	23.01	**0.0001**	1	2.317	0.09	0,7665
AC	1	251.777	2.06	0.1640	1	767.438	29.85	**0.0000**
AD	1	268.772	2.19	0.1510	1	727.234	28.29	**0.0000**
AE	1	25.812	0.21	0.6501	1	6.873	0.27	0.6097
BB	1	46.626	0.38	0.5428	1	165.602	6.44	**0.0178**
BC	1	129.444	1.06	0.3137	1	82.3365	3.20	0.0856
BD	1	58.1581	0.47	0.4971	1	77.844	3.03	0.0941
BE	1	0.365513	0.00	0.9569	1	108.376	4.22	0.0507
CC	1	244.306	2.00	0.1701	1	977.118	38.01	**0.0000**
CD	1	1155.6	9.44	**0.0051**	1	32.623	1.27	0.2706
CE	1	49.6506	0.41	0.5301	1	123.049	4.79	**0.0382**
DD	1	181.68	1.48	0.2346	1	28.8505	1.12	0.2996
DE	1	49.005	0.40	0.5327	1	232.471	9.04	**0.0059**
EE	1	460.953	3.76	0.0637	1	510.629	19.86	**0.0002**

Df = Degree of freedom, MS = Mean square.
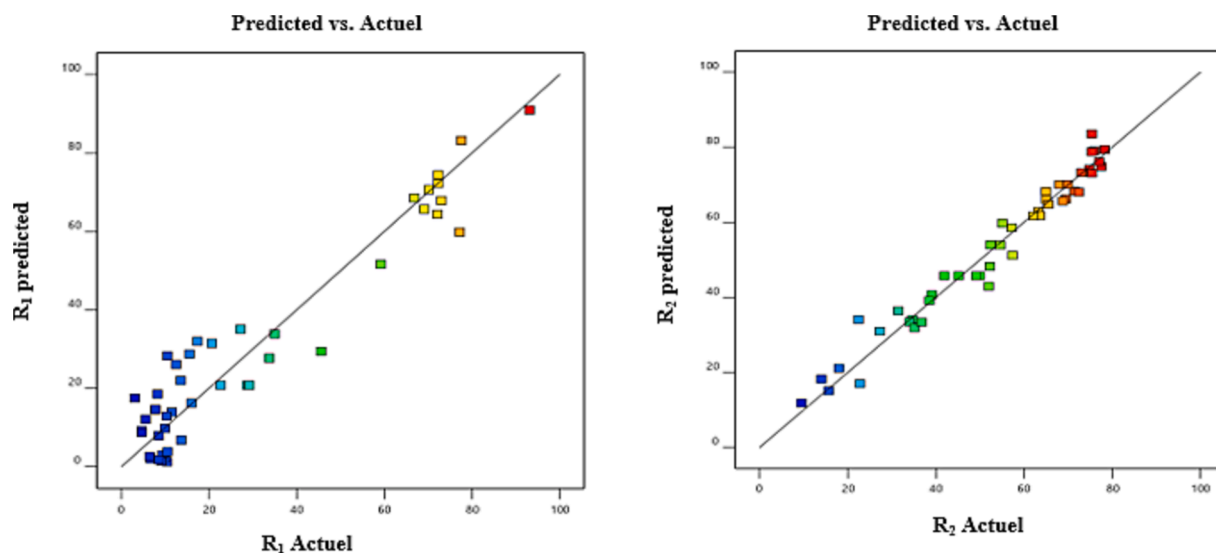
Fig. 13. Predicted values of R_1 and R_2 versus experimental values of R_1 and R_2.

3.5. Study of the factor's effects on the degradation yield of RR-198 by the Fenton process

The effect of the five factors and their interactions on the degradation of the dye is highlighted in Figs. 14 and 15. Based on the Eqs. (6) and (7), the positive sign (+) indicates that an increase in the factor leads to an increase in the degradation of the dye and the interaction has a synergistic effect on the degradation of the dye whereas the negative sign (-) shows that an increase in the factor leads to a decrease in the degradation of the dye and the interaction has an antagonistic effect on the degradation of the dye.

An increase in the factors A, B and D leads to a decrease in the degradation of the dye (Figs. 14 and 15). The effect of initial dye concentration can be explained by the fact that an increase in concentration brings about an increase in the number of dye molecules for the same number of hydroxyl radicals produced. Also, high initial dye concentrations can probably lead to a competitive degradation reaction between the dye molecules and their reaction intermediates in solution. As far as solution pH is concerned, the effect produced in this study shows

that incorporation of magnetite particles into the carbonaceous matrix of BC enables the degradation reaction to by-pass the stringent pH requirements of the homogenous Fenton process. Even though an increase in solution pH induces a decrease in the degradation of the dye, Table 4 shows that the dye can nonetheless be degraded by up to 69.13 % for an initial dye concentration of 62.5 mg/L at pH 5 in the presence of Fe_3O_4-BC1 against 63.68 % for an initial dye concentration of 100 mg/L at pH 8 in the presence of Fe_3O_4-BC2. Therefore, both materials are stable in solution even at pH values greater 4. Wang et al. (2019) reported similar results for the degradation of methylene bleu by the heterogeneous Fenton process in the presence of $_\gamma$-Fe_2O_3-modified graphene oxide sheets. This stability at high pH values can be attributed to the fact that iron-based materials such as magnetite, maghemite and goethite undergo less iron leaching in solution compared to Fe^{2+} in the homogenous Fenton system. Also, these oxides are less susceptible to be precipitated in the form of $Fe(OH)_2$ and $Fe(OH)_3$ compared to Fe^{2+} of the homogeneous Fenton system. However, these results also indicate that Fe_3O_4-BC2 possesses an advantage over Fe_3O_4-BC1, indicating that the co-precipitation method is more efficient than the hydrothermal method
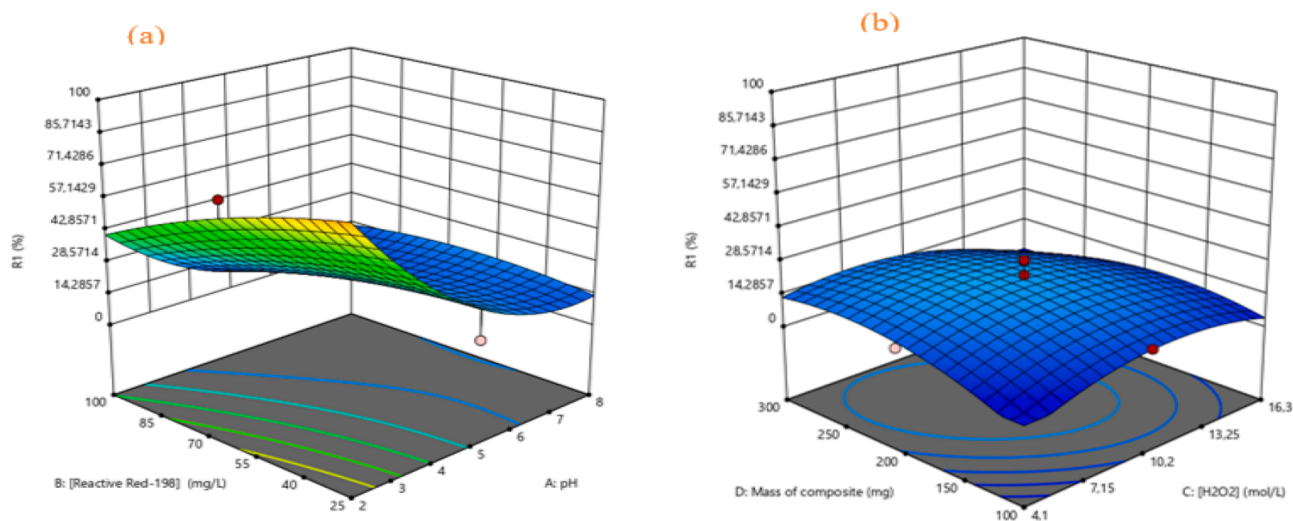
Fig. 14. Surface plots of R_1 illustrating the effects of significant interactions between factors: AB (a) (pH and RR-198 concentration) and CD (b) (concentration of H_2O_2 and mass of composite).
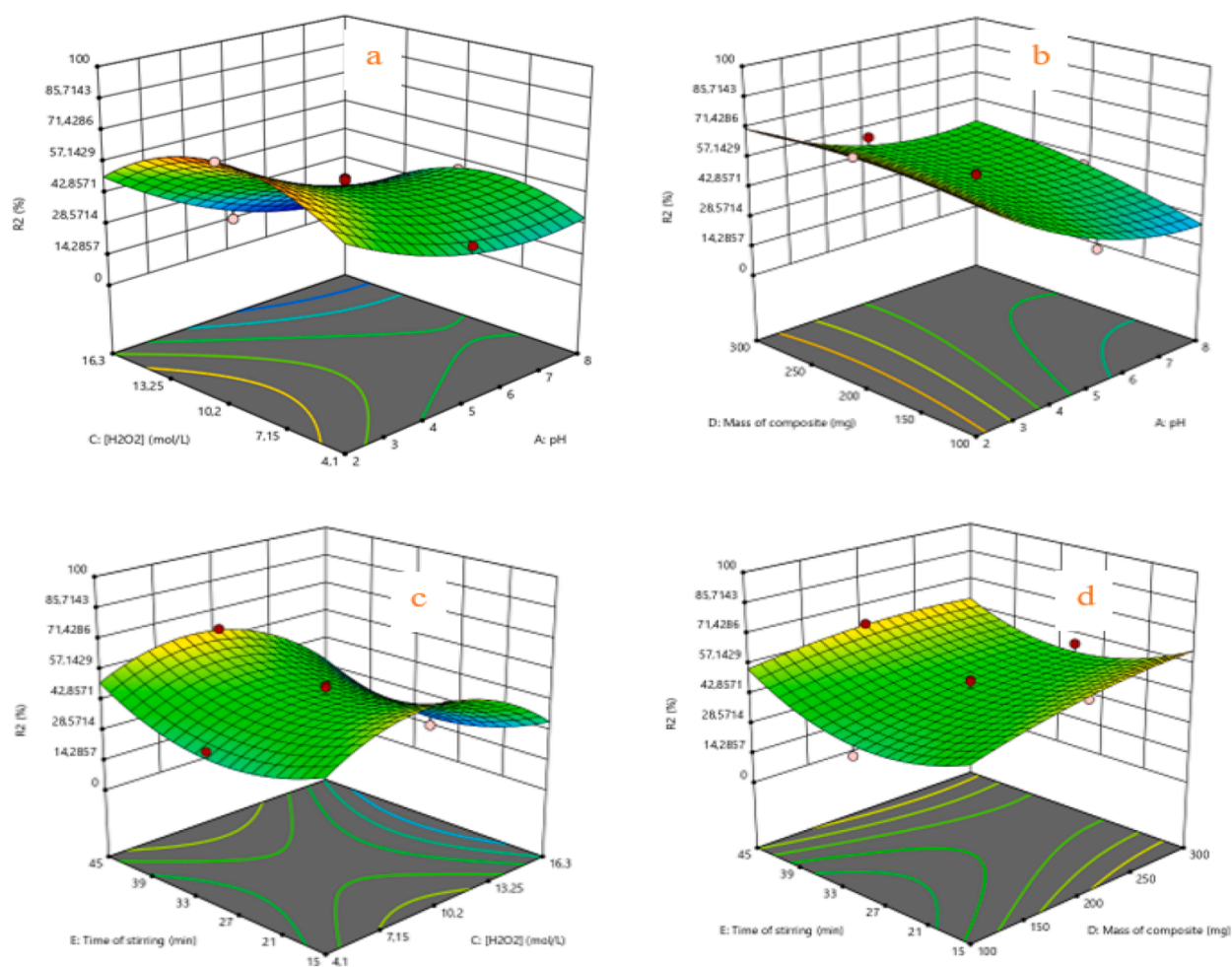
Fig. 15. Surface plots of R_2 illustrating the effects of significant interactions between factors: AC (pH and concentration of H_2O_2), AD (pH and mass of composite), CE (concentration of H_2O_2 and time of stirring) and DE (mass of composite and time of stirring).

of synthesis as earlier suggested by results obtained from FT-IR spectroscopy, SEM and EDX analysis. The effect D suggests that in increase in the mass of the composite material leads to a decrease in the degradation of the dye in the presence of both materials (Figs. 14 and 15). This

perceptible decrease in the dye removal efficiency can be attributed to the fact an increase in the mass of the composite material leads to a corresponding increase in the amount iron species in solution and consequent saturation of the solution. This means during several

elementary steps of the degradation reaction, the excess iron species in solution have a scavenging effect on hydroxyl radicals (Eq. (8)) with potentially negative effect on the efficiency of the degradation reaction (Rubeena et al., 2018).

$$Fe^{2+}(aq) +{}^* OH(aq) \rightarrow Fe^{3+}(aq) + OH^-(aq) \qquad (8)$$
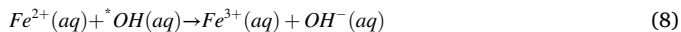
Figs. 14 and 15, also reveal that an increase in factor C brings about a corresponding increase in the dye removal by degradation. Higher concentrations of H_2O_2 generate more hydroxyl radicals in solution that attack the dye molecules at the same time. This ties with results obtained by Panda et al. (2011) for the degradation of methyl orange in aqueous medium using hematite-silica composite material.

3.6. Process optimization of the degradation of RR-198

The optimal conditions for the degradation of the dye in the presence of each composite material alongside the predicted and experimental optimal responses are presented in Table 5. An experimental run was performed at these conditions for degradation of the dye with each composite material and the experimental optimal response obtained was compared to that predicted by the software. Table 5 shows that the responses obtained by experiments under optimal conditions for both composite materials are quite close those predicted by the software. This, in addition to the ANOVA results presented and discussed above confirm the validation of the mathematical model describing the degradation reactions of the dye in the presence of both composite materials.

Under these optimal conditions, Fe_3O_4-BC1 and Fe_3O_4-BC2 both lead to RR-198 degradation yields greater than 90 %. The optimal conditions are acidic in both cases with pH close to 2 as several studies have found optimal conditions in acid zone (Kremer, 2003; Lu et al., 2018; Wypych, 2018). The concentrations of RR-198 and H_2O_2 for Fe_3O_4-BC1 and Fe_3O_4-BC2 are not drastically different as the treatment time and the mass of the composite to be used. The latter for Fe_3O_4-BC1 represents practically the twice that of Fe_3O_4-BC2 while the treatment time of Fe_3O_4-BC1 under optimal conditions represents three times that of Fe_3O_4-BC2, thus illustrating the different behavior of the two composite materials. This, in addition to the results of characterization and the fact that Fe_3O_4-BC2 is more stable at higher pH values further confirm the relative efficiency of the co-precipitation method mover the hydrothermal method for synthesizing magnetite-biochar composite materials. In Table 6, a comparison of the removal efficiency of RR-198 obtained in this work with results found in literature is presented.

3.7. Kinetic studies

The rate constants (k) which are the slopes of the linear plots in Fig. 16 were used to calculate the half-lives of the degradation reactions. Table 7 presents the values of the determination coefficients of the linear kinetic plots and the values of the calculated half-lives. From the values of the determination coefficients, it is evident that the degradation of RR-198 in the presence of Fe_3O_4-BC1 is best described by the first order kinetic rate law ($R^2 = 0.967$) with a half-life of 42.52 min. On the other hand, the second order kinetic rate law is more appropriate for describing the degradation of the dye in the presence of Fe_3O_4-BC2 (R^2

Table 6
Reactive dye removal efficiency reported in literature by various techniques and materials.

Removal technique	Material used	Removal efficiency (%)	Reference
Biodegradation	Microbial strains	80–85 %	Thangaraj et al., 2022
Adsorption	Magnetite nanoparticles	88 %	Deghani et al., 2018
Adsorption	Activated red mud	90 %	Zazouli et al, 2014
Degradation	Fe_3O_4-BC1	93.63	This work
Degradation	Fe_3O_4-BC2	95.48	This work

= 0.986) with a half-life of just 2.019 min. Although the first-order model has a higher coefficient of determination compared to that of the second order for Fe_3O_4-BC1, it would be wiser to take the second-order model for the two composites because this model gives half-reaction times in line with the optimal conditions found. Degradation of the dye in the presence of Fe_3O_4-BC1 needs more time to reach equilibrium contrary to degradation in the presence of Fe_3O_4-BC2 that quickly reaches equilibrium and prolonging the reaction time only leads to the production of undesired products with a consequent antagonistic effect on the response.

3.8. Recovery and reuse of composite materials

The bar graphs in Fig. 17 show the variation in catalytic efficiency of the two composite materials over four consecutive cycles of degradation experiments carried out under optimal conditions for each composite material.

The degradation efficiency of the dye in the presence of Fe_3O_4-BC1 decreases from 93.63 % to 53.56 % after ten cycles of degradation experiments while in the presence of Fe_3O_4-BC2, the decrease is from 95.46 % to 83.97 % after the same number of cycles. This perceptible decrease in the efficiency of Fe_3O_4-BC1 towards degradation of the dye further substantiates the assertion that the co-precipitation method results to a better impregnation of magnetite particles into the carbonaceous matrix of the biochar material as earlier suggested. This also explains the why Fe_3O_4-BC1 is less stable at higher pH values than Fe_3O_4-BC2 and requires more time for the degradation of the dye to reach equilibrium compared to degradation of the dye in the presence of Fe_3O_4-BC2. After ten consecutive cycles of degradation, Fe_3O_4-BC2 loses over 10 % of its catalytic performance whereas Fe_3O_4-BC loses over 40 %. Based on this trend, it can be deduced that Fe_3O_4-BC2 can be used for over 100 cycles under these conditions. This could enhance the industrial applicability of the material in a sustainable and cost-effective manner.

XRD and FT-IR results of the two materials (Fig. 18) recovered from solution after ten consecutive cycles of degradation experiments are identical to the spectra of the materials in Figs. 2 and 3 respectively. Nonetheless, the FT-IR spectrum of Fe_3O_4-BC2 recovered after the adsorption test (Fig. 18b) presents extra bands at 2981, 1382 and 1240 cm^{-1} which are probably due to interferences from the IR transmission patterns of functional groups present dye molecules adsorbed onto the

Table 5
Optimal conditions for the degradation reaction parameters and optimal responses.

Parameter	Optimal value		Optimal response			
	Fe_3O_4-BC1	Fe_3O_4-BC2	Fe_3O_4-BC1		Fe_3O_4-BC2	
			Predicted	Experimental	Predicted	Experimental
A	2.00	2.01	95.71 %	93.63 %	98.38 %	95.48 %
B	25.0 mg/L	26.38 mg/L				
C	8.09 mol/L	9.31 mol/L				
D	243.1 mg	122.48 mg				
E	45 min	15 min				
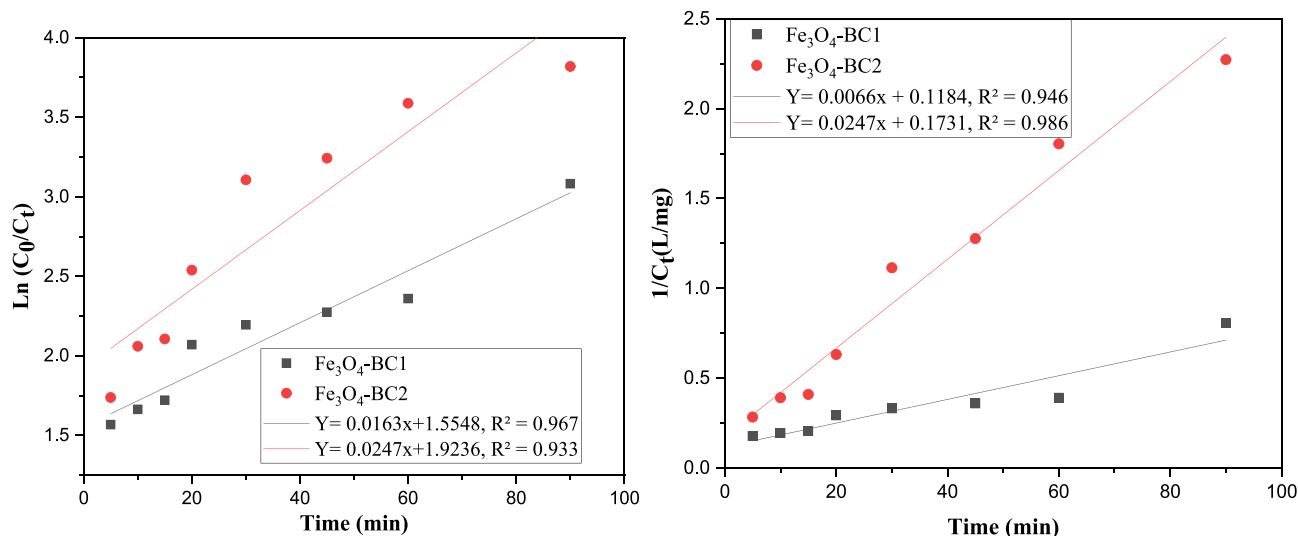
Fig. 16. Linear first order and second order kinetic plots for the degradation reactions in the presence of both composite materials under optimal conditions (solution pH = 2.00, [RR-198 = 25.0 mg/L, [H_2O_2] = 8.09 mol/L, mass of material = 243.1 mg, time = 45 min for Fe_3O_4-BC1 and solution pH = 2.01, [RR-198 = 26.38 mg/L, [H_2O_2] = 9.31 mol/L, mass of material = 122.48 mg, time = 15 min for Fe_3O_4-BC2).

Table 7
Rate constants and calculated half-lives of for the degradation reactions under optimal conditions.

Rate law	Fe_3O_4-BC1			Fe_3O_4-BC2		
	k (min^{-1})	$t_{1/2}$ (min)	R^2	k ($Lmol^{-1}min^{-1}$)	$t_{1/2}$ (min)	R^2
First order	0.0163	42.52	0.967	0.0247	27.949	0.933
Second order	0.0066	5.602	0.946	0.0247	2.0194	0.986

surface of the material. The absence of these bands on the spectrum of Fe_3O_4-BC1 recovered after the adsorption test (Fig. 18b) can be explained by the fact that it adsorbs very little of the dye molecules compared to Fe_3O_4-BC2 (Fig. 11) solutions given its smaller specific surface rea and micropore volume as shown in Table 2.

3.9. Mechanism of degradation

A plausible degradation pathway for reactive red-198 in the presence of *OH is shown in the reaction scheme below. The initial step for the degradation of reactive azo dyes is the reductive cleavage of the —N=N— bond in the presence of *OH. This explains the gradual fading of the red coloration of the dye as soon as the degradation reaction starts given that it is this chromophore that is responsible for the dye's colour in solution. Once the bond is cleaved, P_1 and P_9 are formed. Further attack by *OH on P_1 oxidizes the latter into P_2 and P_3. Since the Fenton reaction is highly favored by acidic conditions, acid hydrolysis of P_3 in solution occurs leading to the formation of $Na_2^+SO_4^{2-}$ and ethanoic acid (P_6). The C—C bond of ethanoic acid is homolytically cleaved and the resulting $CH_3^\bullet$ fragment combines with *OH to from methanol (P_8) while the other fragment forms methanoic acid (P_7). Methanol is further oxidized to methanoic acid and the acidic and oxidizing reaction medium favors the conversion of methanoic acid into to CO_2 and H_2O. At the same time, P_9 is broken down into P_{10} and P_{16}. Splitting of the
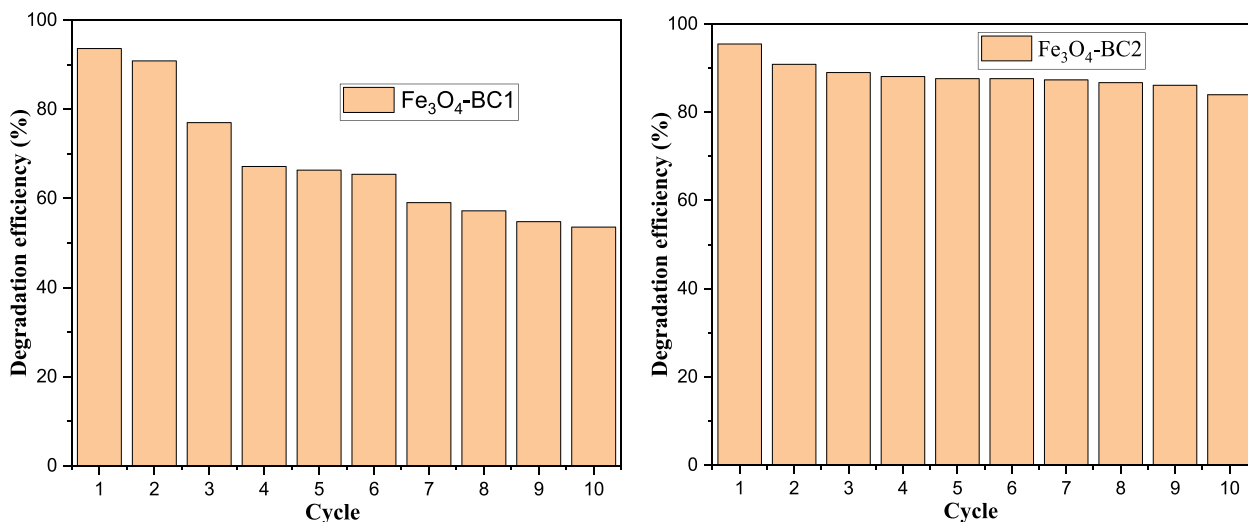
Fig. 17. Change in catalytic efficiency of Fe_3O_4-BC1 and Fe_3O_4-BC2 over four cycles of degradation reactions carried out under the optimal conditions (solution pH = 2.00, [RR-198 = 25.0 mg/L, [H_2O_2] = 8.09 mol/L, mass of material = 243.1 mg, time = 45 min for Fe_3O_4-BC1 and solution pH = 2.01, [RR-198 = 26.38 mg/L, [H_2O_2] = 9.31 mol/L, mass of material = 122.48 mg, time = 15 min for Fe_3O_4-BC2).

naphthalene ring leads to the formation of Buta-1,3-dien-1-ol (P_{18}) and another molecule of P_2. Oxidative cleavage of P_{18} by *OH forms two alkenols (P_{19} and P_{20}). Further oxidation and decomposition of these alkenols yield CO_2 and H_2O as final products of the degradation pathway of P_{18}. Acid hydrolysis of P_{10} generates a chloro-triazin ring (P_{11}) and yet another molecule of P_2. Ring opening of the triazin ring occurs forming P_{12} and P_{13}. P_{13} is oxidized to methanoic acid and eventually CO_2 and H_2O. P_{12} on the other hand, possibly forms a molecule of methamidine

(P_{14}) and methanoyl chloride(P_{15}). Again, the acidic reaction medium favors the formation of methanoic acid from P_{15}, which is in turn oxidized to CO_2 and H_2O and also probably the decomposition of methamidine into molecules of NH_3. The three P_2 molecules undergo oxidative deamination to form P_{22} that undergoes oxidative ring cleavage to afford two molecules of oxo-ethanoic acid and two molecules of methanoic acid that undergo further oxidation into molecules of CO_2 and H_2O.
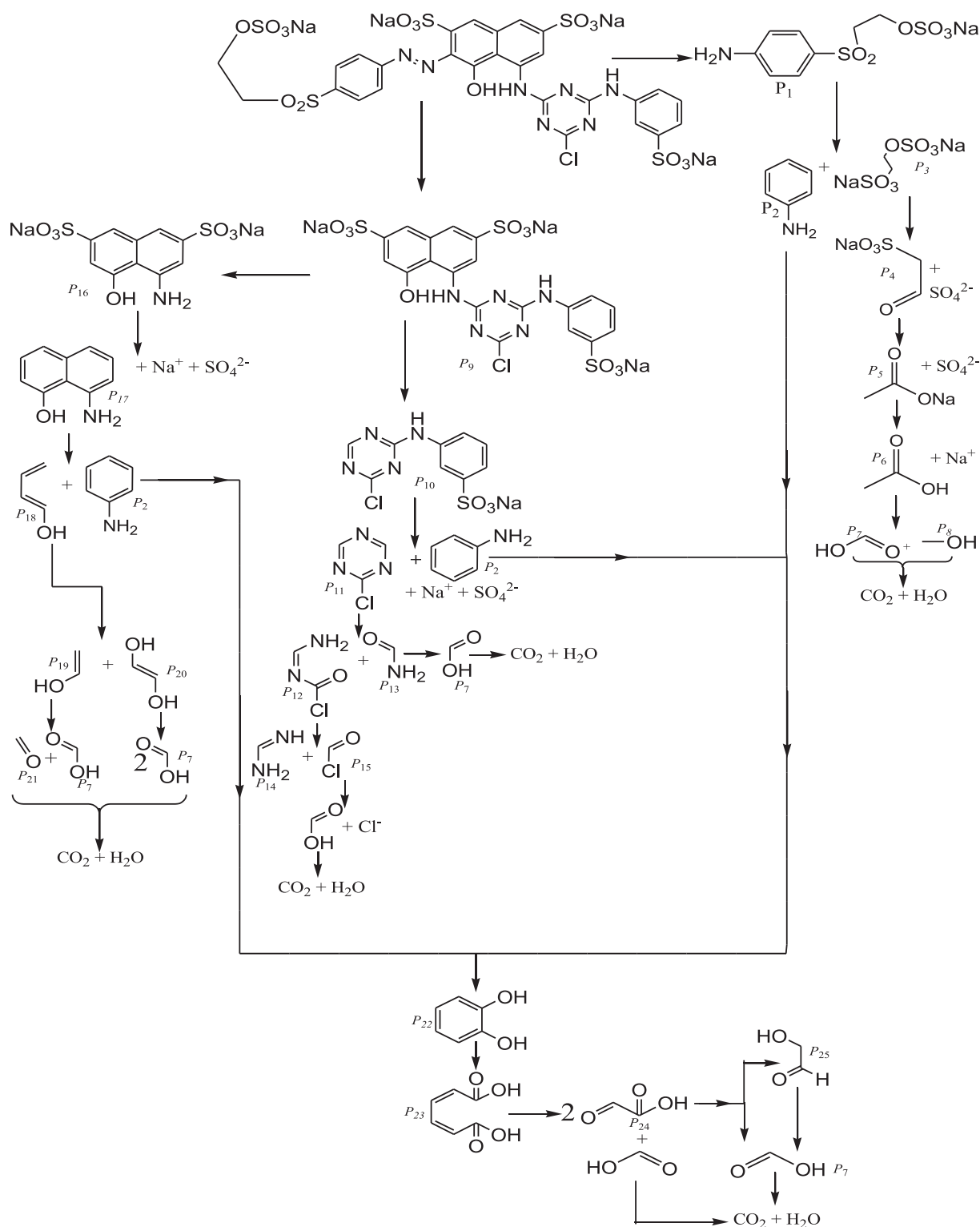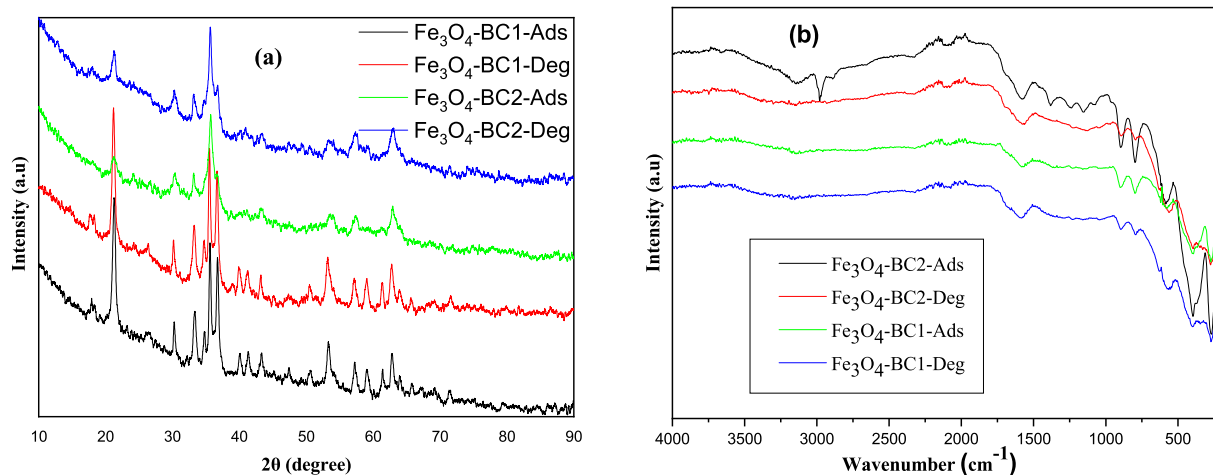
Fig. 18. X-ray diffraction patterns (a) and FT-IR spectra (b) of recovered biochar composite materials after adsorption and degradation experiments.

P = product of degradation: P_1 = sodium-2(4-aminophenylsufonyl) ethylsulfate, P_2 = anline, P_3 = ethane-1,2 disodiumdisulphate, P_4 = ethanalsodiumsulfate, P_5 = sodium ethanoate, P_6 = ethanoic acid, P_7 = methanoic acid, P_8 = methanol, P_9 = sodium 5-(4-amino-6-chloro-1,3,5-triazin-2-ylamino)-4-hydroxynaphthalene-2,7-disulfonate, P_{10} = sodium 3-(4-amino-6-chloro-1,3,5-triazin-2ylamino)benzenesulfonate, P_{11} = 2-Chloro-[1,3,5]triazine, P_{12} = methamidylmethanoylchloride, P_{13} = methanamide, P_{14} = methamidine, P_{15} = methanoylchloride, P_{16} = sodium-3-aminonapthalen-1-ol-5,9-disulfonate, P_{17} = 8-amino-napthalen-1-ol, P_{18} = buta-1,3-dien-1-ol, P_{19} = ethanol, P_{20} = ethene-1,2-diol, P_{21} = methanol, P_{22} = benzene-1,2-diol, P_{23} = *hexa*-2,4-dien-edioic acid, P_{24} = oxo-ethanoic acid, P_{25} = 2-hydroxyethanoic acid.

4. Conclusion

This research focused on optimizing the removal of reactive red-198 by the heterogeneous Fenton process in the presence of two magnetite-biochar composite materials obtained via hydrothermal and co-precipitation methods. The biochar precursor was obtained by pyrolysing of orange peels at 450 °C and subsequently modified using iron salts in alkaline medium. Physico-chemical characterization results showed the presence of iron in the form of mainly Fe_3O_4 present in the carbonaceous matrix of the composite materials obtained via both methods, with some goethite as impurity and also that the co-precipitation method leads to a better impregnation of magnetite particles into the structural matrix of the biochar. The response surface methodology based on the central composite design was used to study the influence of five parameters: dye concentration, solution pH, hydrogen peroxide concentration, mass of composite material and time of stirring on the degradation efficiency of the dye. Optimal conditions resulted to 95.71 and 98.38 % degradation efficiency of the dye in the presence of Fe_3O_4-BC1 and Fe_3O_4-BC2 respectively. Statistical analysis results by ANOVA revealed that two parameters., that is the initial dye concentration and solution pH as well as the interaction between these two parameters significantly influence the degradation of the dye in the presence of both materials. Moreso, Fe_3O_4-BC2 shows higher stability at elevated pH values compared to Fe_3O_4-BC1 as far as the heterogeneous Fenton process is concerned. ANOVA results also demonstrate a good correlation between the experimental or actual and predicted values of the response. The first and second order kinetic rate laws were used to study the degradation of the dye and it resulted that the second order rate law best describes the process in the presence of both composite materials. Finally, the catalytic efficiency of the two materials was tested over ten cycles of dye degradation experiments. Both materials demonstrate appreciable stability over the cycles but again Fe_3O_4-BC2 retains its catalytic efficiency much more than Fe_3O_4-BC1.

Availability of data and material

All data cited in this work are available.

Code availability

'Not applicable'.

Declaration of competing interest

The authors declare that they have no known competing financial interests or personal relationships that could have appeared to influence the work reported in this paper.

Acknowledgements

References

Abdelaal, A., Pradhan, S., Alnouss, A., Tong, Y., Al-Ansari, T., McKay, G., Mackey, H.R., 2021. The impact of pyrolysis conditions on orange peel biochar physicochemical properties for sandy soil. Waste. Manage. Res. 39, 995–1004. https://doi.org/10.1177/0734242x20978456.

Abdelhafez, A.A., Li, J., 2016. Removal of Pb (II) from aqueous solution by using biochars derived from sugar cane bagasse and orange peel. J. Taiwan Inst Chem. Eng. 61, 367–375. https://doi.org/10.1016/j.tice.2016.01.005.

Adeniyi, A.G., Ighalo, J.O., Onifade, D.V., 2020. Biochar from the thermochemical conversion of orange (Citrus sinensis) peel and albedo: product quality and potential applications. Chem. Afr. 3, 439–448. https://doi.org/10.1007/s42250-020-00119-6.

Adeniyi, A.G., Iwuozor, K.O., Emenike, E.C., Ogunniyi, S., Amoloye, M.A., Sagboye, P.A., 2023. One-step chemical activation for the production of engineered orange peel biochar. Emerge. Mat. 6, 211–221. https://doi.org/10.1007/s42247-022-00442-3.

Ai, T., Jiang, X., Zhong, Z., Li, D., Dai, S., 2020. Methanol-modified ultra-fine magnetic orange peel powder biochar as an effective adsorbent for removal of ibuprofen and sulfamethoxazole from water. Adsopt. Sci. Technol. 38, 304–321. https://doi.org/10.1177/0263617420944659.

Amin, M.T., Alazba, A.A., Shafiq, M., 2019. Comparative study for adsorption of methylene blue dye on biochar derived from orange peel and banana biomass in aqueous solutions. Environ. Monit. Assess. 191, 1–14. https://doi.org/10.1007/s10661-019-7915-0.

Armynah, B., Atika, D.Z., Piarah, W.H., Tahir, D., 2018. Analysis of chemical and physical properties of biochar from rice husk biomass. J. Phys. Conf. Ser. 979, 012038 https://doi.org/10.1088/1742-6596/979/012038.

Bezerra, M.A., Santelli, R.E., Oliveira, E.P., Villar, L.S., Escaleira, L.A., 2008. Response surface methodology (RSM) as a tool for optimization in analytical chemistry. Talanta 76, 965. https://doi.org/10.1016/j.talanta.2008.05.019.

Bopda, A., Mafo, S.G.M., Ndongmo, J.N., Kenda, G.T., Fotsop, C.G., Kuete, I.-H.-T., Ngakou, C.S., Tchuifon, D.R.T., Tamo, A.K., Nche, G.-N.-A., Anagho, S.G., 2022. Ferromagnetic biochar prepared from hydrothermally modified calcined mango seeds for Fenton-like degradation of indigo carmine. J. Carbon Res. 8, 81. https://doi.org/10.3390/c8040081.

Chaki, S.H., Tasmira, J.M., Chaudhary, M.D., Tailor, J.P., Deshpande, M.P., 2015. Magnetite nanoparticles synthesis by wet chemical reduction and their characterization. Adv. Nat. Sci.: Nanosci. Naonotechnol. 6, 32–40. https://doi.org/10.1088/2043-6262/6/3/035009.

Chen, B., Chen, Z., 2009. Sorption of naphthalene and 1-naphthol by biochars of orange peels with different pyrolytic temperatures. Chemosphere 76, 127–133. https://doi.org/10.1016/j.chemosphere.2009.02.004.

Chen, B., Chen, Z., Lv, S., 2011. A novel magnetic biochar efficiently sorbs organic pollutants and phosphate. Bioresour. Technol. 102, 716–723. https://doi.org/10.1016/j.biortech.2010.08.067.

Dehghani, M.H., Pourshabanian, M., Heidarinejad, Z., 2018. Experimental data on the adsorption of reactive red 198 from aqueous solution using Fe_3O_4 nanoparticles: optimization by response surface methodology with central composite design. Data Brief 19, 2126–2132. https://doi.org/10.1016/j.dib.2018.07.008.

Enders, A., Hanley, K., Whitman, T., Joseph, S., Lehmann, J., 2012. Characterization of biochars to evaluate recalcitrance and agronomic performance. Bioresour. Technol. 114, 644–653. https://doi.org/10.1016/j.biortech.2012.03.022.

Fenton, H.J., 1984. Oxidation of tartaric acid in the presence of ferrous iron. J. Chem. Soc. 65, 889–910. https://doi.org/10.1039/CT8946500899.

Fernandez, M., Gorria, P., Blanco, J., Fuertes, B., Sevilla, M., Boada, R., Chaboy, J., Schmool, D., Greneche, J., 2010. Microstructure and magnetism of nanoparticles with $^{\gamma}$-Fe core surrounded by α-Fe and iron oxide shells. Phys. Rev. B 81, 1–10. https://doi.org/10.1103/PhysRevB.81.0.

Gareth, D., James, M., 2021. Hydrothermal synthesis of biomass-derived magnetic carbon composites for adsorption and catalysis. ACS Omega 6, 48–67. https://doi.org/10.1021/acsomega.1c05116.

Gupta, V.K., Ali, I., 2013. In: Environmental Water: Advances in Treatment, Remediation and Recycling, second ed. Elsevier, Oxford. https://doi.org/10.1016/C2011-0-05782-4.

Herney-Ramirez, J., Vicente, M., Madeira, L., 2010. Heterogeneous photo-Fenton oxidation with pillared clay-based catalysts for wastewater treatment: a review. Appl. Catal. b. Environ. 98, 10–26. https://doi.org/10.1016/j.apcatb.2010.05.004.

Jiang, J., Xu, R.K., Jiang, T.Y., Li, Z., 2012. Immobilization of Cu(II), Pb(II) and Cd(II) by the addition of rice straw derived biochar to a simulated polluted ultisol. J. Hazard. Mater. 229–230, 145–150. https://doi.org/10.1016/j.hazmat.2012.05.086.

Jung, Y.S., Lim, W.T., Park, J.Y., Kim, Y.H., 2009. Effect of pH on Fenton and Fenton-like oxidation. Environ. Technol. 30, 183–190. https://doi.org/10.1080/09593338602468848.

Katibi, K.K., Yunos, K.F., Man, H.C., Aris, A.Z., Nor, M.Z., Azis, R.S., 2021. An insight into a sustainable removal of bisphenol A from aqueous solution by novel palm kernel shell magnetically induced biochar: synthesis, characterization, kinetic and thermodynamic studies. Polymers 13, 37–81. https://doi.org/10.3390/polym13213781.

Khelifi, S., Ayari, F., Hassan, C.D., Chehimi, D.B., Trabelsi-Ayadi, M., 2016. Synthesis and characterization of heterogeneous catalysts and comparison to iron-ore. J. Chem. Eng. Process Technol. 7, 316. https://doi.org/10.4172/2157-7048.1000316.

Kremer, M.L., 2003. The Fenton Reaction: dependence of the rate on pH. J. Phy. Chem. A 107, 1734–1741. https://doi.org/10.1021/jp020654p.

Li, S., Zhang, G., Zhang, W., Zheng, H., Zhu, W., Sun, N., Zheng, Y., Wang, P., 2017. Microwave enhanced Fenton-like process for degradation of perfluorooctanoic acid (PFOA) using Pb-BiFeO3/rGO as heterogeneous catalyst. Chem. Eng. J. 326, 756–764. https://doi.org/10.1016/j.cej.2017.06.037.

Liu, N., Charrua, A.B., Weng, C.-H., Yuan, X., Ding, F., 2015. Characterization of biochars derived from agriculture wastes and their adsorptive removal of atrazine from aqueous solution: a comparative study. Bioresour. Technol. 198, 55–62. https://doi.org/10.1016/j.biortech.2015.08.129.

Lu, J., Chen, R., Liang, H., Yan, Q., 2018. The influence of concentration of hydroxyl radical on the chemical mechanical polishing of SiC wafer based on the Fenton reaction. Process. Eng. 52, 221–226. https://doi.org/10.1016/j.precisioneng.2017.12.011.

Mady, A.H., Baynosa, M.L., Tuma, D., Shim, J.J., 2017. Facile microwave-assisted green synthesis of Ag-ZnFe2O4 @rGO nanocomposites for efficient removal of organic under UV- and visible-light irradiation. Appl. Catal. B Environ. 203, 416–427. https://doi.org/10.1016/j.apcatb.2016.10.033.

Mafo, S.G., Tchuifon, D.R., Ngakou, C.S., Fotsop, C.G., Kouteu, P.A., Doungmo, G., Ndifor-Angwafor, N.G., Anagho, S.G., 2023. Study of the degradation of Bezaktiv Brilliant Blue by the Fenton process using a prepared ferromagnetic activated carbon

from rubber seed hull as heterogeneous catalyst. Desalin. Water Treat. 2023, 1–14. https://doi.org/10.5004/dwt.2023.29358.

Mahmoud, M.E., Abouelanwar, M.E., Mahmoud, S.E.M.E., Abdel Salam, M., 2022. Adsorption behavior of silver quantum dots by a novel super magnetic CoFe2O4-biochar-polymeric nanocomposite. J. Colloid Interface Sci. 606, 1597–1608. https://doi.org/10.1016/j.jcis.2021.08.102.

Makela, M., 2017. Experimental design and response surface methodology in energy applications: a tutorial review. Energy Convers. Manage. 151, 630–640. https://doi.org/10.1016/j.encoman.2017.09.021.

Meng, F., Yang, B., Wang, B., Duan, S., Chen, Z., Ma, W., 2017. Novel dendrimerlike magnetic biosorbent based on modified orange peel waste: adsorption–reduction behavior of arsenic. ACS Sustain. Chem. Eng. 5, 9692–9700. https://doi.org/10.1021/acssuschemeng.7b01273.

MINADER, 2015. The state of biodiversity for food and agriculture in the Republic of Cameroon, first ed. Ministry of Agriculture and Rural Development, Yaounde, Cameroon.

Navalon, S., Alvaro, M., Garcia, H., 2010. Heterogenous Fenton catalysts based on clays, silicas and zeolites. Appl. Catal. B-Environ. 99, 1–26. https://doi.org/10.1016/j.chemosphere.2004.09.080.

Ngankam, S., Lemankreo, D., Baissassou, D., Abdellaziz, B., Abdelrani, Y., Abdoul, N., 2020. Preparation and characterization of magnetic banana peels biochar for Fenton degradation of methylene blue. Mater. Sci. Appl. 11, 382–400. https://doi.org/10.4236/msa.2020.116026.

Panda, N., Sahoo, H., Mohapatra, S., 2011. Decolourization of methyl orange using Fenton like mesoporous Fe2O3-SiO2 composite. J. Hazard. Mater. 185 (1), 359–365. https://doi.org/10.1016/j.jhazmat.2010.09.042.

Pearce, C.I., Lloyd, J.R., Guthrie, J.T., 2003. The removal of colour from textile wastewater using whole bacterial cells: a review. Dyes Pigment. 58, 179–196. https://doi.org/10.1016/so143-7208(03)00064-0.

Peng, Z., Fan, Z., Chen, X., Zhou, X., Gao, Z.F., Deng, S., Wan, S., Lv, X., Shi, Y., Han, W., 2022. Fabrication of nano iron oxide-modified biochar from co-hydrothermal carbonization of microalgae and Fe(II) salt for efficient removal of rhodamine B. Nanomaterials 12, 2271. https://doi.org/10.3390/nanao12132271.

Plakas, K.V., Karabelas, A.J., 2016. A study on heterogeneous Fenton regeneration of powdered activated carbon impregnated with iron oxide nanoparticles. Glob. Nest J. 18, 259–268. https://doi.org/10.30955/gnj.001894.

Raghavan, V., Basha, S.J., Jegan, J., 2013. Review on efficacious methods to decolorize reactive azo dye. J. Urban Environ. Eng. 7, 30–47. https://doi.org/10.40901/juee.2013.v7n1.030047.

Rubeena, K.K., Reddy, P.R., Laiju, A.R., Nideesh, P.V., 2018. Iron impregnated biochars as heterogeneous Fenton catalyst for the degradation of acid red 1 dye. J. Environ. Manage 226, 320–328. https://doi.org/10.1016/j.jenvman.2018.08.055.

Thangaraj, S., Bankole, P.O., Sadasivam, S.K., Kumarvel, V., 2022. Biodegradation of Reactive Red 198 by textile effluent adapted microbial strains. Archives Microbio. 204 (12), 1–13. https://doi.org/10.1007/s00203-021-02608-9.

Thommes, M., Kaneko, K., Neimark, A.V., Olivier, J.P., Rodriguez-Reinoso, F., Rouquerol, J., Sing, K.S.W., 2015. Physisorption of gases, with special reference to the evaluation of surface area and pore size distribution (IUPAC Technical Report). Pure Appl. Chem. 87, 1051–1069.

Tong, X.J., Li, J.Y., Yuan, J.H., Xu, R.K., 2011. Adsorption of Cu(II) by biochars generated from three crop straws. Chem. Eng. J. 172, 828–834. https://doi.org/10.1016/j.cej.2011.06.069.

Wang, F., Yu, X., Ge, M., Wu, S., Guan, J., Tang, J., Wu, X., Robert, O., 2019. Facile self-assembly synthesis of $^{\gamma}$-Fe2O3/graphene oxide for enhanced photo-Fenton reaction. Environ. Pollut. 248, 229–237. https://doi.org/10.1016/j.envpol.2019.01.018.

Wypych, G., 2018. Photochemistry. In: Wypych, G. (Ed.), Handbook of Material Weathering, sixth ed. ChemTec Publishing, Toronto, pp. 27–49. https://doi.org/10.1016/B978-1-927885-31-4.50004-2.

Ying, D., Hong, P., Jiali, F., Qinqin, T., Yuhui, L., Youqun, W., Zhibin, Z., Xiaohong, C., Yunhai, L., 2020. Removal of uranium using MnO2/orange peel biochar composite prepared by activation and in-situ deposition in a single step. Biomass Bioenergy 142, 105772. https://doi.org/10.1016/j.biombioe.2020.105772.

Zazouli, M.A., Balarak, D., Mahdavi, Y., Ebrahimi, M., 2014. Adsorption rate of 198 reactive red dye from aqoues solutions by using activated red mud. Iranian J. Health Sci. 1 (1), 36–43. https://doi.org/10.18869/acadpub.jhs.1.1.36.

Zhang, W., Wang, Y., Fan, L., Liu, X., Cao, W., Ai, H., Wang, Z., Liu, X., Jia, H., 2022. Sorbent properties of orange peel-based biochar for different pollutants in water. Processes 10, 856. https://doi.org/10.3390/pr10050856.

Zhou, W., Rajic, L., Chen, L., Kou, K., Ding, Y., Meng, X., Wang, Y., Mulaw, B., Gao, J., Qin, Y., Alshawabkeh, A.N., 2019. Activated carbon as effective cathode material in iron-free electro-Fenton process: integrated H_2O_2 electrogeneration, activation, and pollutants adsorption. Electrochim. Acta 296, 317–326. https://doi.org/10.1016/j.elecacta.2018.11.052.